JOURNAL OF GEOPHYSICAL RESEARCH, VOL. 114, D22303, doi:10.1029/2009JD012123, 2009

Click Here for Full Article

Retrieval of vertical columns of sulfur dioxide from SCIAMACHY and OMI: Air mass factor algorithm development, validation, and error analysis

Chulkyu Lee,[1] Randall V. Martin,[1,2] Aaron van Donkelaar,[1] Gray O'Byrne,[1] Nickolay Krotkov,[3] Andreas Richter,[4] L. Gregory Huey,[5] and John S. Holloway[6,7]

Received 25 March 2009; revised 19 June 2009; accepted 6 August 2009; published 18 November 2009.

[1] We develop an improved retrieval of sulfur dioxide (SO_2) vertical columns from two satellite instruments (SCIAMACHY and OMI) that measure ultraviolet solar backscatter. For each SCIAMACHY and OMI observation, a local air mass factor (AMF) algorithm converts line-of-sight "slant" columns to vertical columns using altitude-dependent scattering weights computed with a radiative transfer model (LIDORT), weighted by relative vertical SO_2 profile (shape factor) determined locally with a global atmospheric chemistry model (GEOS-Chem). The scattering weights account for viewing geometry, surface albedo, cloud scattering, absorption by ozone, and scattering and absorption by aerosols. Absorption of radiation by mineral dust can reduce seasonal mean instrument sensitivity by 50%. Mean SO_2 shape factors simulated with GEOS-Chem and used in the AMF calculation are highly consistent with airborne in situ measurements (INTEX-A and INTEX-B); differences would affect the retrieved SO_2 columns by 10%. The retrieved vertical columns are validated with coincident airborne in situ measurements (INTEX-A, INTEX-B, and a campaign over east China). The annual mean AMF errors are estimated to be 35–70% in polluted regions (e.g., East Asia and the eastern United States) and less than 10% over clear ocean regions. The overall SO_2 error assessment is 45–80% for yearly averages over polluted regions. Seasonal mean SO_2 columns retrieved from SCIAMACHY and OMI for 2006 are significantly spatially correlated with those from GEOS-Chem, in particular over the United States (r = 0.85 for SCIAMACHY and 0.82 for OMI). A sensitivity study confirms the sensitivity of SCIAMACHY and OMI to anthropogenic SO_2 emissions.

Citation: Lee, C., R. V. Martin, A. van Donkelaar, G. O'Byrne, N. Krotkov, A. Richter, L. G. Huey, and J. S. Holloway (2009), Retrieval of vertical columns of sulfur dioxide from SCIAMACHY and OMI: Air mass factor algorithm development, validation, and error analysis, *J. Geophys. Res.*, *114*, D22303, doi:10.1029/2009JD012123.

1. Introduction

[2] Sulfur dioxide (SO_2) is released into the atmosphere as a result of both anthropogenic activities and natural (e.g., volcanic, phytoplankton) phenomena. SO_2 oxidizes rapidly in the atmosphere, leading to aerosol formation and acid deposition. Aerosols have highly uncertain effects on climate [*Intergovernmental Panel on Climate Change* (*IPCC*), 2007; *Climate Change Science Program* (*CCSP*), 2009], are deleterious to human health, and degrade visibility. Outstanding questions exist about SO_2 emissions [*Streets and Waldhoff*, 2000] and its atmospheric chemistry and meteorological mechanisms of long-range transport [*Dickerson et al.*, 2007]. Global mapping of atmospheric SO_2 concentrations can provide critical information on its emissions and transport and generally improve scientific understanding of SO_2 atmospheric chemistry.

[3] Satellite remote sensing using spectral fitting techniques has been employed for the measurement of atmospheric trace species on global and regional scales [*Chance*, 2005; *Fishman et al.*, 2008]. SO_2 observation from space was first performed using the Total Ozone Mapping Spectrometer (TOMS) [*Krueger*, 1983]. The TOMS sensitivity to SO_2 was limited by its limited wavelength coverage to large SO_2 amounts in volcanic eruptions and exceptional SO_2 pollution events [e.g., *Krueger et al.*, 1995; *Carn et al.*, 2004]. More recently, SO_2 retrievals with greatly improved

[1]Department of Physics and Atmospheric Science, Dalhousie University, Halifax, Nova Scotia, Canada.
[2]Harvard-Smithsonian Center for Astrophysics, Cambridge, Massachusetts, USA.
[3]Goddard Earth Sciences and Technology Center, University of Maryland, Baltimore County, Baltimore, Maryland, USA.
[4]Institute of Environmental Physics and Remote Sensing, University of Bremen, Bremen, Germany.
[5]School of Earth and Atmospheric Sciences, Georgia Institute of Technology, Atlanta, Georgia, USA.
[6]Cooperative Institute for Research in Environmental Science, University of Colorado at Boulder, Boulder, Colorado, USA.
[7]Chemical Science Division, Earth System Research Laboratory, NOAA, Boulder, Colorado, USA.

Copyright 2009 by the American Geophysical Union.
0148-0227/09/2009JD012123$09.00

Table 1. Specifications of SCIAMACHY and OMI

Instrument	Satellite Platform	Measurement Period	Equator Crossing Time, Local Time	Spectral Range (nm)	Spectral Resolution (nm)	Spatial Resolution (Nadir) (km)	Global Coverage (days)	Viewing Zenith Angles (deg)
SCIAMACHY	Envisat	2002–present	1000	220–2400	0.25–0.4	30 × 60	6	5–20
OMI	EOS-Aura	2004–present	1330	270–500	0.5	13 × 24	1	<65

sensitivity have been achieved using ultraviolet (UV) hyperspectral data available from a new generation of satellite spectrometers such as the Global Ozone Monitoring Experiment (GOME) [e.g., *Eisinger and Burrows*, 1998; *Khokhar et al.*, 2005; *Thomas et al.*, 2005], Scanning Imaging Absorption Spectrometer for Atmospheric Chartography (SCIAMACHY; Table 1) [e.g., *Afe et al.*, 2004; *Richter et al.*, 2006; *Lee et al.*, 2008b], and Ozone Measurement Instrument (OMI; Table 1) [e.g., *Krotkov et al.*, 2006, 2008; *Carn et al.*, 2007; *Yang et al.*, 2007]. However, a major challenge remains in the derivation of quantitative vertical column amounts. Moreover, little is known about the consistency of satellite SO_2 retrievals with simulated columns and in situ measurements.

[4] An air mass factor (AMF) is required for the conversion of the retrieved line-of-sight "slant" column into a vertical column. The SO_2 AMF depends critically on the vertical distribution of SO_2, surface albedo, viewing geometry, clouds, aerosol profile and optical properties, and the ozone (O_3) column [*Khokhar et al.*, 2005; *Thomas et al.*, 2005; *Richter et al.*, 2006; *Krotkov et al.*, 2008]. *Khokhar et al.* [2005] applied a global uniform AMF of unity to GOME measurements of volcanic SO_2, assuming a surface albedo of 3%, aerosol optical depth of 0.1, an SO_2 plume height 4–5 km, and an overhead cloud fraction of 20%. *Thomas et al.* [2005] developed an AMF algorithm for GOME volcanic SO_2 measurements, including scattering by clouds and the SO_2 profile. *Lee et al.* [2008a] applied an AMF of 0.88 to their SCIAMACHY SO_2 retrieval over East Asia, based on a surface albedo of 3%, maritime aerosol loading, and a polluted SO_2 vertical profile. The operational OMI planetary boundary layer (PBL) SO_2 product assumes a globally uniform AMF of 0.36 calculated for cloud- and aerosol-free conditions, a solar zenith angle (SZA) of 30°, a surface albedo of 5%, a midlatitude ozone profile, and a typical summer SO_2 vertical profile over the eastern United States [*Taubman et al.*, 2006]. *Krotkov et al.* [2008] examined a correction to the operational AMF over China using aircraft measurements of polluted SO_2 and aerosol profiles [*Dickerson et al.*, 2007] and OMI total ozone. In the SO_2 data of the Tropospheric Emission Monitoring Internet Service (TEMIS, http://www.temis.nl/), the AMF is taken from a look-up table determined using inputs such as SZA, the surface albedo, cloud fraction and cloud top pressure, and a set of SO_2 profiles that depend on the SO_2 column, assuming a constant ozone amount of 350 DU (Dobson Unit, 1 DU $\approx 2.69 \times 10^{16}$ molecules cm^{-2}).

[5] The AMF calculation in our work combines a radiative transfer model with spatially varying geophysical fields. We extend the AMF formulation of *Palmer et al.* [2001] and *Martin et al.* [2002] to tropospheric SO_2 retrieved from SCIAMACHY and OMI. Vertical shape factors (relative vertical distribution) for SO_2 are locally determined with a global 3-D model of tropospheric chemistry (GEOS-Chem). Our AMF calculation accounts for scattering by clouds using local cloud fraction and cloud pressure determined from SCIAMACHY and OMI measurements. Local surface reflectivity is from a 14 year TOMS UV reflectivity climatology [*Herman and Celarier*, 1997]. Total column O_3 is from SCIAMACHY and OMI. Aerosols are from a global GEOS-Chem simulation. The retrieved SO_2 columns and the shape factor used in the AMF calculation are validated with airborne in situ measurements over North America and the North Atlantic Ocean collected during the aircraft campaigns of Intercontinental Chemical Transport Experiment–Phase A (INTEX-A) from June to August 2004 [*Singh et al.*, 2006] and over the United States and Mexico during Phase B (INTEX-B) from March to May 2006 [*Singh et al.*, 2009].

[6] Section 2 describes the atmospheric chemistry model (GEOS-Chem) used in this work. Section 3 develops the AMF formulation, compares the SO_2 simulated relative vertical distribution with that of airborne in situ measurements, and examines the effects of atmospheric ozone and aerosol on the seasonal variation of AMF. In section 4, we present SO_2 slant and vertical columns retrieved from SCIAMACHY and OMI, validate the retrieved SO_2 vertical columns with airborne in situ profile measurements during INTEX-A and INTEX-B, and compare them to the GEOS-Chem columns. Section 5 discusses errors in the retrievals. Sensitivity of the retrieved SO_2 columns to emissions is examined in section 6.

2. Atmospheric Chemistry Model

[7] Retrieving tropospheric SO_2 vertical columns from solar backscatter observations requires local information about the vertical distribution of SO_2. A global 3-D model of tropospheric chemistry is the best source of this information considering the sparseness of in situ measurements and the large variability of SO_2 vertical profiles. We use the GEOS-Chem chemical transport model v8-01-04 [*Bey et al.*, 2001] (http://acmg.seas.harvard.edu/geos/) to obtain the SO_2 vertical distribution. GEOS-Chem is a global 3-D model of tropospheric chemistry driven by assimilated meteorological observations from the Goddard Earth Observing System (GEOS-4) at the NASA Goddard Global Modeling Assimilation Office (GMAO: http://gmao.gsfc.nasa.gov/). The GEOS-Chem model version used here has 30 vertical levels on a pressure-based, terrain-following eta (η) coordinate and horizontal resolution of 2° latitude by 2.5° longitude.

[8] The GEOS-Chem model includes a detailed simulation of the aerosol-oxidant system. The aerosol simulation in GEOS-Chem includes the sulfate-nitrate-ammonium system [*Park et al.*, 2004], carbonaceous aerosols [*Park et al.*,

Table 2. Annual Global Sulfur Emissions in the GEOS-Chem Model for the Year 2006

Source	Emission Rate (Tg S yr^{-1})
Fossil fuel on land	51.55
Ships	4.72
Biomass burning	1.22
Biofuel burning	0.12
Aircraft	0.07
Volcano	6.55
Dimethyl sulfide (DMS)	21.05

2003], sea salt [*Alexander et al.*, 2005], and mineral dust [*Fairlie et al.*, 2007]. The aerosol and oxidant simulations are coupled through formation of sulfate and nitrate [*Park et al.*, 2004], heterogeneous chemistry [*Jacob*, 2000], and aerosol effects on photolysis rates [*Martin et al.*, 2003b]. The optical properties for mineral dust used for the standard GEOS-Chem simulation are based on the refractive indices of *Patterson et al.* [1977]. There is growing recognition that those values are too absorbing at UV wavelengths [*Colarco et al.*, 2002]. We use a Mie algorithm [*de Rooij and van der Stap*, 1984; *Mishchenko et al.*, 1999] to recalculate the optical properties of mineral dust based on the refractive indices of *Sinyuk et al.* [2003]; the single scattering albedo at 300 nm of mineral dust in GEOS-Chem increases by 0.14 to the range of 0.7–0.9.

[9] The model uses detailed emission inventories, including recent updates by *van Donkelaar et al.* [2008]. Table 2 contains the annual global sulfur emissions used in the model. The global anthropogenic emission inventory for NO_x, SO_x, and CO is based on EDGAR [*Olivier et al.*, 2001] for the base year of 2000. The global inventory is replaced with regional inventories from NEI99 (http://www.epa.gov/ttn/chief/net/1999inventory.html) over the United States for 1999, BRAVO [*Kuhns et al.*, 2005] over Mexico for 1999, CAC (http://www.ec.gc.ca/pdb/cac/cac_home_e.cfm) over Canada for 2005, Streets [*Zhang et al.*, 2009] for eastern Asia for 2006, and EMEP (http://www.emep.int) over Europe for 2005. We scale all regional and global inventories from their respective base year to 2004, the last year of available statistics, unless its base year is after 2004. The EDGAR ship emission inventory yielded AMFs with sharply defined ship tracks that are inconsistent with the satellite data. We replace the EDGAR ship emission inventory with the International Comprehensive Ocean-Atmosphere Data Set (ICOADS) [*C. Wang et al.*, 2008].

[10] Natural sources of sulfur in the model include volcanoes and atmospheric oxidation of dimethyl sulfide (DMS) from phytoplankton. The oceanic water emission of DMS is calculated as the product of local seawater DMS concentration and sea-to-air transfer velocity [*Park et al.*, 2004]. Volcanic emissions of SO_2 from continuously active and sporadically erupting volcanoes are included from the database of *Andres and Kasgnoc* [1998]. We update the inventory for 2006 following *Chin and Jacob* [1996] using the database of the Global Volcanism Program (GVP: http://www.volcano.si.edu/). The total amount of SO_2 emitted by a given eruption, and the height of the eruption plume, are specified as function of the volcanic explosivity index [*Newhall and Self*, 1982; *Simkin and Siebert*, 1994].

[11] The GEOS-Chem sulfur simulation has been evaluated in a number of previous studies. GEOS-Chem generally gives unbiased simulation of sulfate aerosol concentrations over North America [*Park et al.*, 2004; *Heald et al.*, 2006]. *Park et al.* [2004] and *van Donkelaar et al.* [2008] found that the model can reproduce with no significant bias the observed vertical profiles of SO_x from the TRACE-P and INTEX-B aircraft campaigns, although there is evidence that SO_2 oxidation may be too rapid [*Heald et al.*, 2006; *van Donkelaar et al.*, 2008]. The United States SO_x emission inventory used in the simulation is believed to be well defined [*Park et al.*, 2004; *Heald et al.*, 2006; *van Donkelaar et al.*, 2008].

[12] We conduct simulations for the years 2004 and 2006. The GEOS-Chem output is averaged within 0900 to 1100 local time (LT) and 1300 to 1500 LT to cover the SCIAMACHY and OMI overpasses for use in the AMF calculation and subsequent analysis.

3. AMF Calculation

[13] Here we develop a local AMF formulation for SO_2 and apply it to SCIAMACHY and OMI observations.

3.1. AMF Formulation

[14] The AMF is defined as the ratio of the slant column of an optically thin absorber along an average backscattered path observed by a satellite instrument, to the vertical column. In the absence of scattering for a plane parallel atmosphere, the AMF is a geometric air mass factor AMF_G, which is a simple function of the solar zenith angle θ_s and the satellite instrument viewing zenith angle θ_v

$$\mathrm{AMF}_G = \sec(\theta_s) + \sec(\theta_v). \tag{1}$$

[15] Due to atmospheric Rayleigh and Mie scattering, the AMF is sensitive to the relative vertical distribution of the absorber. The AMF calculation applied here is based on the formulation of *Palmer et al.* [2001] and *Martin et al.* [2002] for the retrieval of HCHO and NO_2 from GOME measurements. A dimensionless vertical shape factor $S(\eta)$ representing a normalized vertical profile of mixing ratio over the eta (η) vertical coordinate, is determined from the GEOS-Chem simulation for each observation pixel

$$S(\eta) = C(\eta)\frac{\Omega_{air}}{\Omega_{SO2}}, \tag{2}$$

where $C(\eta)$ is the SO_2 mixing ratio, and Ω_{air} and Ω_{SO2} are the vertical columns of air and SO_2 from surface to the model top (0.01 hPa).

[16] Scattering weights $\omega(\eta)$ describe the vertically resolved instrument sensitivity to SO_2. More specifically $\omega(\eta)$ is the sensitivity of the dimensionless solar normalized radiance I observed by a satellite instrument to local variation of the abundance of SO_2 at each level η.

$$\omega(\eta) = -\frac{1}{\mathrm{AMF}_G}\frac{\alpha(\eta)}{\alpha_e}\frac{\partial(\ln I)}{\partial\tau}, \tag{3}$$

where $\alpha(\eta)$ is the temperature-dependent absorption cross section (cm^2 $molecules^{-1}$), α_e is the effective absorption

cross section (cm^2 $molecules^{-1}$) representing an average cross section weighted by the vertical distribution of SO_2 in the column [*Palmer et al.*, 2001], and $\partial\tau$ is the optical depth increment of SO_2 as a function of η. AMF_G normalizes the scattering weights such that $\omega(\eta) = 1$ in a nonscattering atmosphere. Local temperature vertical profiles are from GEOS-4. We assume that the slant optical depth of the layer can be given by the product of the vertical optical depth and the average light path enhancement. The AMF is then written as [*Palmer et al.*, 2001]

$$\mathrm{AMF} = \mathrm{AMF}_G \int_0^1 \omega(\eta) S(\eta) d\eta. \tag{4}$$

[17] The AMF formulation accounts for cloud-contaminated pixels, which are typical in satellite measurements, using the cloud information (e.g., cloud fraction and cloud pressure) following *Martin et al.* [2002]. The effective cloud fraction and cloud pressure for our AMF calculation are from FRESCO+ [*P. Wang et al.*, 2008] for SCIAMACHY and the OMCLDRR [*Joiner and Vasilkov*, 2006] for OMI. Surface reflectivity is from a 14 year climatology from TOMS at 360 nm [*Herman and Celarier*, 1997]. Local O_3 columns are from SCIAMACHY and OMI as discussed in section 3.3. Local aerosol profiles are from GEOS-Chem as discussed in section 3.4. The U.S. summer standard ozone profile is used in the AMF calculation. Using local O_3 profiles from GEOS-Chem changes the AMF by <2%. Scattering weights for both the clear and cloudy fractions of the pixel are calculated using the Linearized Discrete Ordinate Radiative Transfer (LIDORT) radiative transfer model [*Spurr et al.*, 2001; *Spurr*, 2002].

[18] The cloud radiance fraction c, the fraction of the radiance from the cloudy sky subpixel, can be expressed as

$$c = \frac{f \cdot R_{cloud}}{f \cdot R_{cloud} + (1-f) \cdot R_{clear}}, \tag{5}$$

where f is the effective cloud fraction ($0 \le f \le 1$), and the reflectivity of the clear R_{clear} and cloudy R_{cloud} scene is obtained from the radiative transfer model and measured reflectance. AMFs are first calculated for the clear AMF_{clear} and cloudy AMF_{cloud} fractions, assuming the same shape factor in each subpixel. The combined AMF accounting for clouds is then given by

$$\mathrm{AMF} = (1-c) \cdot \mathrm{AMF}_{clear} + c \cdot \mathrm{AMF}_{cloud} \tag{6}$$

[19] The AMF significantly depends on wavelength as Rayleigh scattering increases at shorter wavelengths and can be different for SO_2 slant column retrievals from SCIAMACHY and OMI [*Thomas et al.*, 2005; *Richter et al.*, 2006]. We calculate the AMF at 319.7 nm for SCIAMACHY SO_2 and at 313.2 nm for OMI SO_2, the middle of the fit wavelength ranges for the corresponding slant column retrievals (section 4.1).

[20] Figure 1 (left) shows the global distribution of the seasonal mean AMF for OMI SO_2. The AMF tends to be largest over ocean, reflecting the higher center of mass pressure (CMP) of SO_2 over ocean, and the greater instrument sensitivity to SO_2 in the free troposphere. Smaller AMFs over polluted regions indicate reduced instrument sensitivity to SO_2 in the boundary layer. The AMFs over the eastern United States and China are similar (~0.5) reflecting similar CMP of ~910 hPa (0.9 km) of the SO_2 profile [*Krotkov et al.*, 2008]. Relatively high AMF values are found over continental regions that have high surface reflectivity or are intensely convective. The seasonal variation in the AMF over the high-latitude oceans arises largely from the seasonal variation in solar zenith angle. Except for regions of biomass burning (e.g., central Africa and central South America), the seasonal variation in the AMF over land is less pronounced, due to the weak seasonal variation in shape factors and scattering weights in the boundary layer. The seasonal AMFs for SCIAMACHY are up to 25% higher than those shown for OMI over ocean and up to 25% lower than those shown for OMI over land, reflecting in both cases the larger solar zenith angles of SCIAMACHY morning observations. The slight diurnal variation in the SO_2 profile also contributes to the lower SCIAMACHY AMFs over land due to the shallow boundary layer in morning that increases the SO_2 CMP.

3.2. Shape Factors

[21] Here we evaluate the relative vertical profile (shape factor) of SO_2 used in the AMF calculation. Figure 2 shows aircraft flight tracks of the NASA DC-8 and the NSF C-130 for INTEX-A and INTEX-B used for the evaluation. Flight conditions range from remote marine to highly polluted regions. The DC-8 sampled over the eastern United States and the North Atlantic Ocean for INTEX-A, and over Hawaii and Mexico for INTEX-B. The C-130 sampled over the northwestern United States and Mexico for INTEX-B. SO_2 was measured in situ on the DC-8 by chemical ionization mass spectrometry [*Kim et al.*, 2007], and on the C-130 by UV pulsed fluorescence [*Ryerson et al.*, 1998]. The comparisons exclude fresh pollution plumes as diagnosed by $NO_x/NO_y > 0.4$ mol mol^{-1} or (if NO_y is not available) $NO_2 > 4$ ppbv and altitude <2 km; biomass burning plumes as diagnosed by HCN > 500 pptv or $CH_3CN > 225$ pptv or flight logs; and stratospheric air as diagnosed by $O_3/CO > 1.25$ mol mol^{-1} [*Hudman et al.*, 2007].

[22] Figure 3 compares shape factors of SO_2 inferred from airborne in situ measurements with those calculated with the GEOS-Chem simulation as used in our AMF calculation. The GEOS-Chem simulation for these comparisons is sampled along aircraft flight tracks at observation time. Shape factor vertical profiles depend on the pressure level of the SO_2 source. The shape factors for INTEX-A (Figure 3, top) exhibit a maximum in the boundary layer due to regional pollution and outflow. The SO_2 gradient in the boundary layer reflects averaging over multiple flights. Shape factors for INTEX-B generally correspond to cleaner conditions, with the exception of Mexico City outflow near 700 hPa. The simulated SO_2 profiles near the top of the boundary layer tend to exhibit a positive bias that is similar, albeit smaller, than found by *Hains* [2007] who compared CMAQ and GOCART SO_2 profiles versus aircraft measurements over the eastern United States. The airborne measurements and model calculations are highly consistent providing confidence in the AMF calculation, and in the ability of the GEOS-Chem model to represent SO_2 vertical

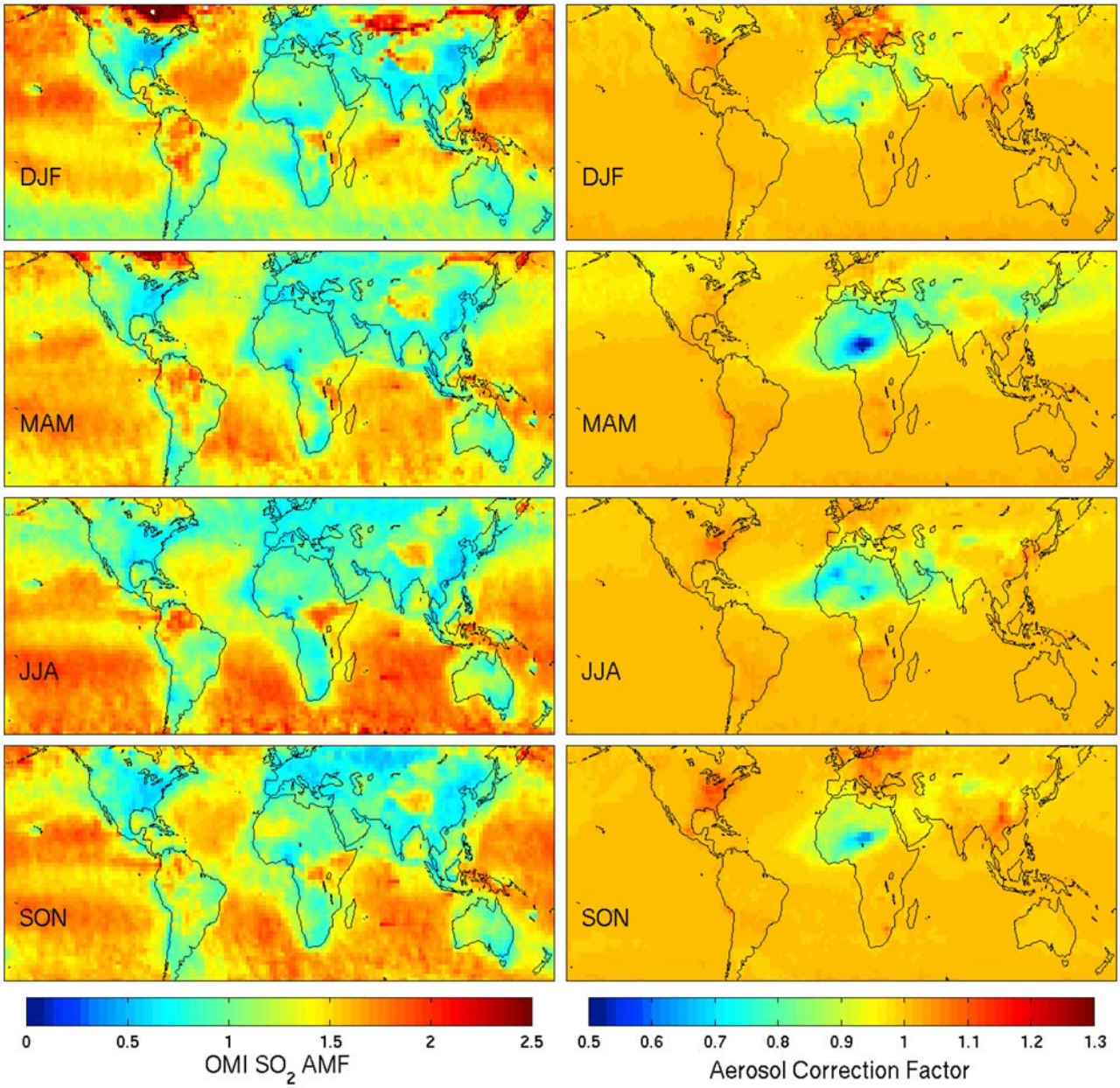

Figure 1. (left) Air mass factor (AMF) for conversion of slant to vertical SO_2 columns in the OMI measurements. (right) The aerosol correction factors relative to an AMF calculation without aerosols (see section 3.4). Values are seasonal means for December–February (DJF), March–May (MAM), June–August (JJA), and September–November (SON) for the year 2006.

profiles. The AMF calculated from the campaign-averaged in situ profile is typically within 10% of the AMF determined from simulated profiles. The largest discrepancy occurs over northwestern United States (NWUS in Figure 3), where the AMF calculated with the measured profile is 14% higher than the AMF calculated with the simulated profile. The error in the simulated profiles is much smaller than the ~100% error that would arise from using a global uniform vertical profile of SO_2 in the AMF calculation [e.g., *Khokhar et al.*, 2005; *Thomas et al.*, 2005]. The simulated profile shape can significantly reduce the uncertainty in the AMF calculation.

3.3. Ozone Correction

[23] Our AMF calculation accounts for absorption of UV radiation by ozone using an O_3 vertical profile S_{O3} in the scattering weight calculation (equation 3) that is scaled by the total ozone column $T_{O3,sat}$ of the coincident satellite observation pixel

$$S_{O3}(\sigma) = C_{O3}(\sigma)\frac{T_{O3,sat}}{T_{O3,US}}, \tag{7}$$

where C_{O3} is the U.S. summer standard ozone profile and $T_{O3,U.S.}$ is the corresponding total column of 311 DU. Total

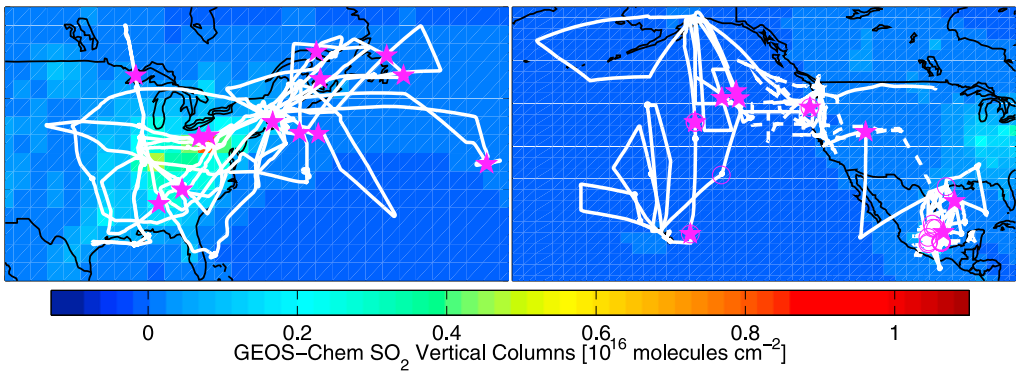

Figure 2. Location of aircraft measurements used for evaluation. White solid lines indicate the flight tracks of the NASA DC-8. Dotted lines indicate flight tracks for the NSF C-130 aircraft. The location of coincident aircraft and satellite measurements are indicated with magenta stars for SCIAMACHY and magenta circles for OMI, respectively. The background image is of SO_2 columns calculated with the GEOS-Chem model for (left) July–August 2004 INTEX-A and (right) April–May 2006 during INTEX-B.

O_3 columns of SCIAMACHY and OMI used here are from the WFDOAS retrieval [*Weber et al.*, 2007] and the OMI TOMS-V8 total O_3 algorithm [*Bhartia and Wellemeyer*, 2002], respectively.

[24] The magnitude of the effect increases with the O_3 slant column [*Krotkov et al.*, 2008]. The O_3 effect on the AMF can be large (>30%) for certain conditions (i.e., large O_3 vertical column, solar zenith angle, and viewing zenith angle), but can be accounted for accurately using satellite-measured total O_3 in equations (4)–(7). The ozone correction to the SCIAMACHY SO_2 AMF is 10–20% smaller than for OMI, reflecting wavelength dependence of O_3 absorption.

3.4. Aerosol Correction

[25] Scattering and absorption by aerosols have significant effects on satellite retrievals of atmospheric trace gases [e.g., *Torres and Bhartia*, 1999; *Colarco et al.*, 2002; *Sinyuk et al.*, 2003; *Torres et al.*, 2007]. *Krotkov et al.* [2008] compared in situ aircraft measurements and OMI SO_2 retrievals to infer the sensitivity of OMI SO_2 retrievals to different types of UV-absorbing aerosols. Following *Martin et al.* [2003a], we account for aerosols in the AMF calculation by representing within the LIDORT model their vertically resolved optical properties from the GEOS-Chem simulation described in section 2. These same aerosol fields (sulfate, size-resolved mineral dust and sea salt, hydrophobic and hydrophilic black carbon, and hydrophobic and hydrophilic organic carbon) also are used to account for the effect of aerosols on photolysis frequencies and heterogeneous chemistry in the GEOS-Chem model [*Martin et al.*, 2003b; *Evans and Jacob*, 2005; *Sauvage et al.*, 2007].

[26] Figure 1 (right) shows the aerosol correction factor. UV-absorbing dust reduces the AMF by up to 50% over the Sahara during MAM and by 15–30% over the Middle East and Central Asia. In Northern Hemisphere spring, dust transport from the deserts of central Asia decreases the AMF over northeast Asia. Scattering aerosols increase the AMF by <15% over industrial regions such as the eastern United States and Western Europe. However, these AMF increases should be taken with caution, since recent ground measurements have shown enhanced UV absorption for typical suburban summer aerosols in the eastern United States [*Krotkov et al.*, 2005] and for pollution aerosols downwind of Mexico City [*Barnard et al.*, 2008; *Corr et al.*, 2009], which would result in reduced AMFs. Additional direct measurements of aerosol optical properties at UV wavelengths would better constrain the modeled aerosol correction. The correction factors for aerosol to the SCIAMACHY SO_2 AMF are within 15% of those for OMI.

4. Vertical Columns of SO_2

[27] Here we describe the SO_2 columns retrieved from SCIAMACHY and OMI, and compare them to values simulated with GEOS-Chem.

4.1. Slant Columns

[28] The SO_2 slant column retrieval for SCIAMACHY is based on the algorithms (Differential Optical Absorption Spectroscopy) of *Afe et al.* [2004], *Richter et al.* [2006], and *Lee et al.* [2008a, 2008b]. The wavelength range of 315–327 nm is used for the SO_2 fit. In addition to the SO_2 cross section (295K) [*Vandaele et al.*, 1994], two ozone cross sections (223K and 243K) [*Bogumil et al.*, 2003], a synthetic Ring spectrum [*Vountas et al.*, 1998], an undersampling correction, and the polarization dependence of the SCIAMACHY instrument are included in the fit. Daily solar irradiance measurements taken with the ASM diffuser are used as the reference spectra. We use here the data taken at SZA < 70° and cloud radiance fraction < 0.2.

[29] Figure 4a shows the mean SCIAMACHY SO_2 slant columns for 2006. Pronounced enhancements are found over volcanoes and industrial regions in China. There is no evidence of SO_2 column enhancements along ship tracks, in contrast with NO_2 [*Beirle et al.*, 2004; *Richter et al.*, 2004]. Large scatter in the South Atlantic Anomaly (SAA) region over South America and the Southern Atlantic Ocean results from reduced signal-to-noise due to exposure of the low-orbiting satellite instrument to radiation and particles. Figure 4b shows the zonal mean slant columns over the Pacific. SO_2 slant columns have a latitude-dependent offset, which could be related to imperfect corrections for ozone interference and the Ring effect [*Van Roozendael et al.*, 2002; *Lee et al.*, 2008b].

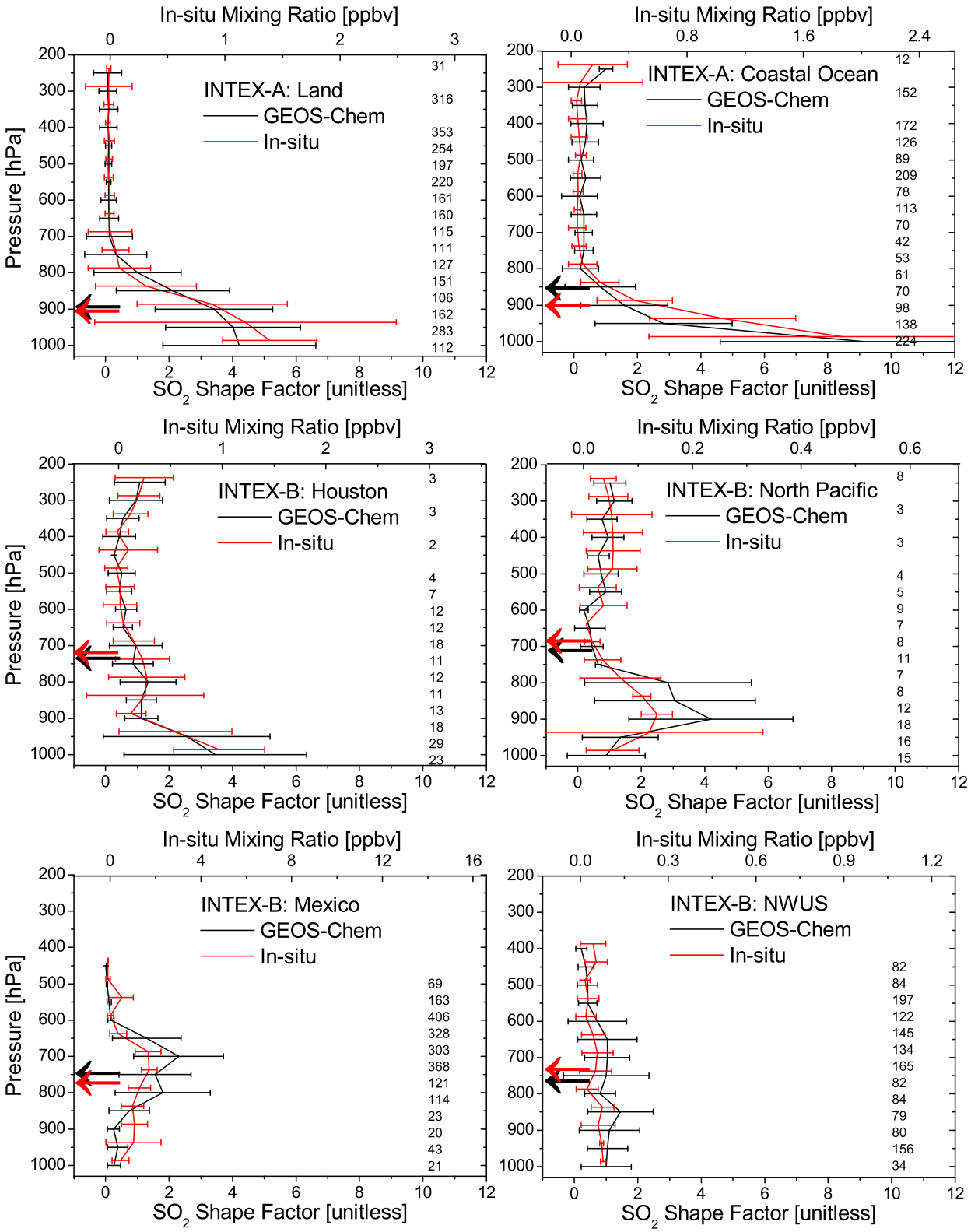

Figure 3. Shape factors (relative vertical distribution) of SO_2 over land and ocean of the eastern United States and North Atlantic Ocean averaged over the entire INTEX-A period, and over Houston (20°N–33°N, 100°W–91°W), the North Pacific (40°N–61°N, 151°W–140°W), Mexico (18°N–22°N, 102°W–90°W), and the northwest United States (38°N–50°N, 133°W–122°W) over the entire INTEX-B period. The red and black lines show the shape factors (equation (2)) determined from in situ measurements and the GEOS-Chem model, respectively. The number of measurements (n) within each 50 hPa interval is shown in the right of each plot. Error bars represent the standard deviations divided by $\sqrt{n}$. Center of mass pressure is indicated with arrows in black for simulated profiles and in red for in situ measurements.

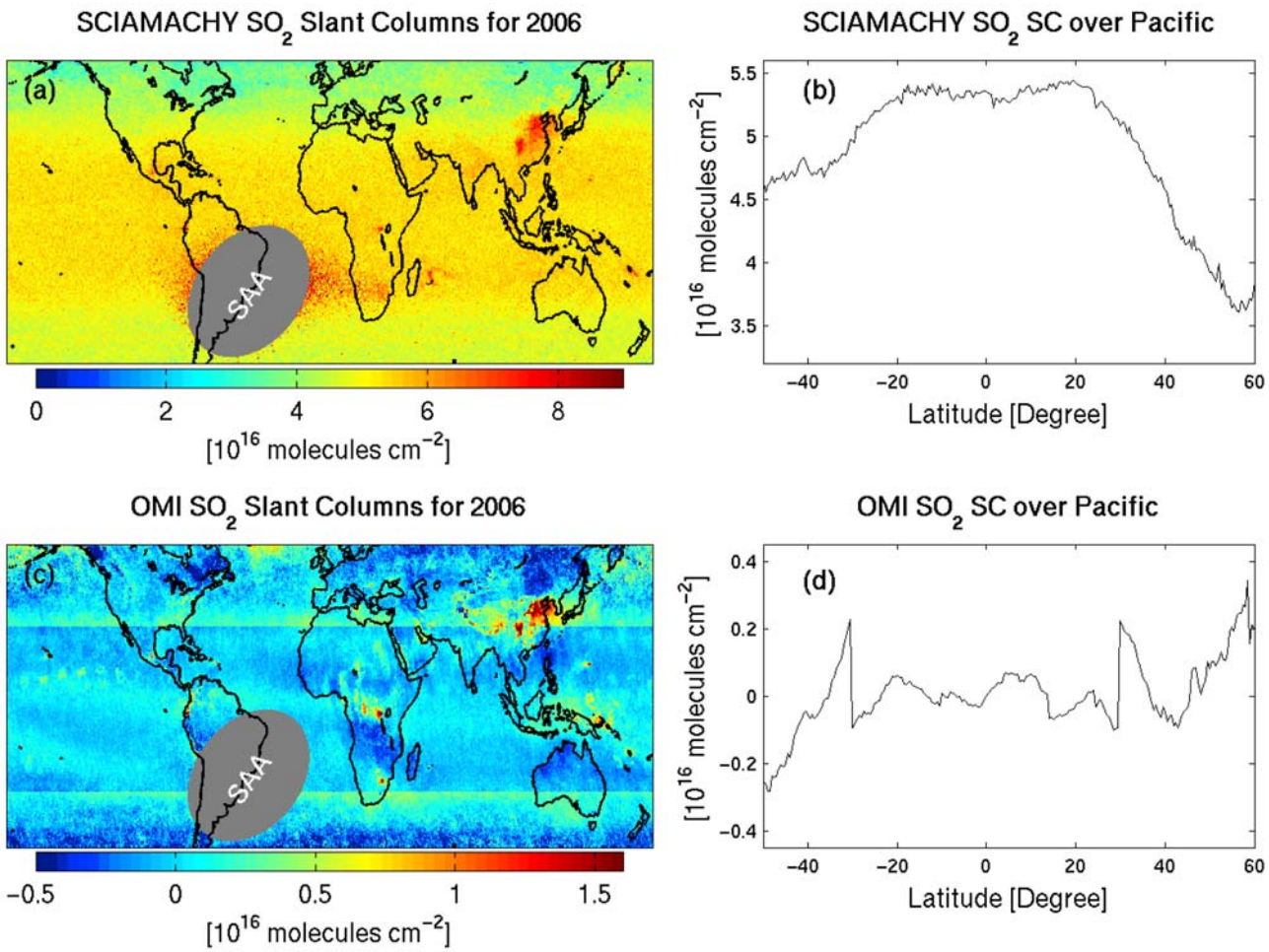

Figure 4. (left) Global map of SO_2 slant columns (SC) from (a) SCIAMACHY and (c) OMI averaged for 2006. SO_2 SC data are the output of the spectral fit and have constant and latitudinal varying offsets. (right) SO_2 SC in the reference sector over the Pacific region which is denoted by white lines in Figure 5 from (b) SCIAMACHY and (d) OMI. SO_2 data are screened in the area of the Southern Atlantic Anomaly (SAA), where large scatter in retrieved SO_2 results from exposure of the instruments to radiation and particles.

[30] For OMI we use the publicly released Planetary Boundary Layer (PBL) OMI SO_2 Level 2 product retrieved with the Band Residual Difference algorithm [*Krotkov et al.*, 2006, 2008]. The algorithm is a two step retrieval. First, the OMI TOMS-V8 algorithm [*Bhartia and Wellemeyer*, 2002] retrieves the total ozone amount by matching the calculated radiances to the measured radiances at a pair of wavelengths (317.5 and 331.2 nm) assuming no SO_2 and using cloud pressures from OMCLDRR [*Joiner and Vasilkov*, 2006]. The residuals at 10 other wavelengths are then calculated as the difference between the measured and computed radiances including 4 short UV wavelengths in the SO_2 bands: 310.8, 311.9, 313.2, and 314.4 nm. In the presence of SO_2, the residuals contain spectral structures that correlate with the SO_2 absorption cross sections. A 'sliding median' empirical correction is used to reduce any cross-track and meridional biases, which subtracts a median residual for a sliding group of SO_2 free pixels and minimal cloud contamination (OMTO3 radiative cloud fraction < 0.15) covering ± 15° latitude along the orbit track from each spectral band and cross-track position [*Yang et al.*, 2007, *Krotkov et al.*, 2008]. Second, the SO_2 algorithm (OMSO2) converts corrected differential residuals at the three wavelength pairs with the largest differential SO_2 cross sections in the OMI UV2 spectral region (P1 = 310.8–311.9; P2 = 311.9–313.2, and P3 = 313.2–314.4 nm) to the SO_2 slant columns differential SO_2 cross-sections data at constant temperature (275 K) [*Bogumil et al.*, 2003]. The slant columns of the three pairs are averaged and the average slant column is converted to the total SO_2 vertical column by dividing by a constant AMF of 0.36.

[31] We converted the OMI PBL SO_2 vertical columns back to slant columns by multiplying by the original constant AMF of 0.36. We use here the data with near-nadir viewing angles (cross-track position from 20 to 40) at SZA < 70° and cloud radiance fraction < 0.2.

[32] Figure 4c shows the mean OMI SO_2 slant columns for 2006. Enhancements exist over volcanoes and East Asia. No enhancement is found over ship tracks. The data have a negative offset and a sharp gradient (<6 × 10^{15} molecules cm^{-2}) at ± 30° latitude, as seen in Figure 4d. The gradient at ± 30° latitude is caused by the residual

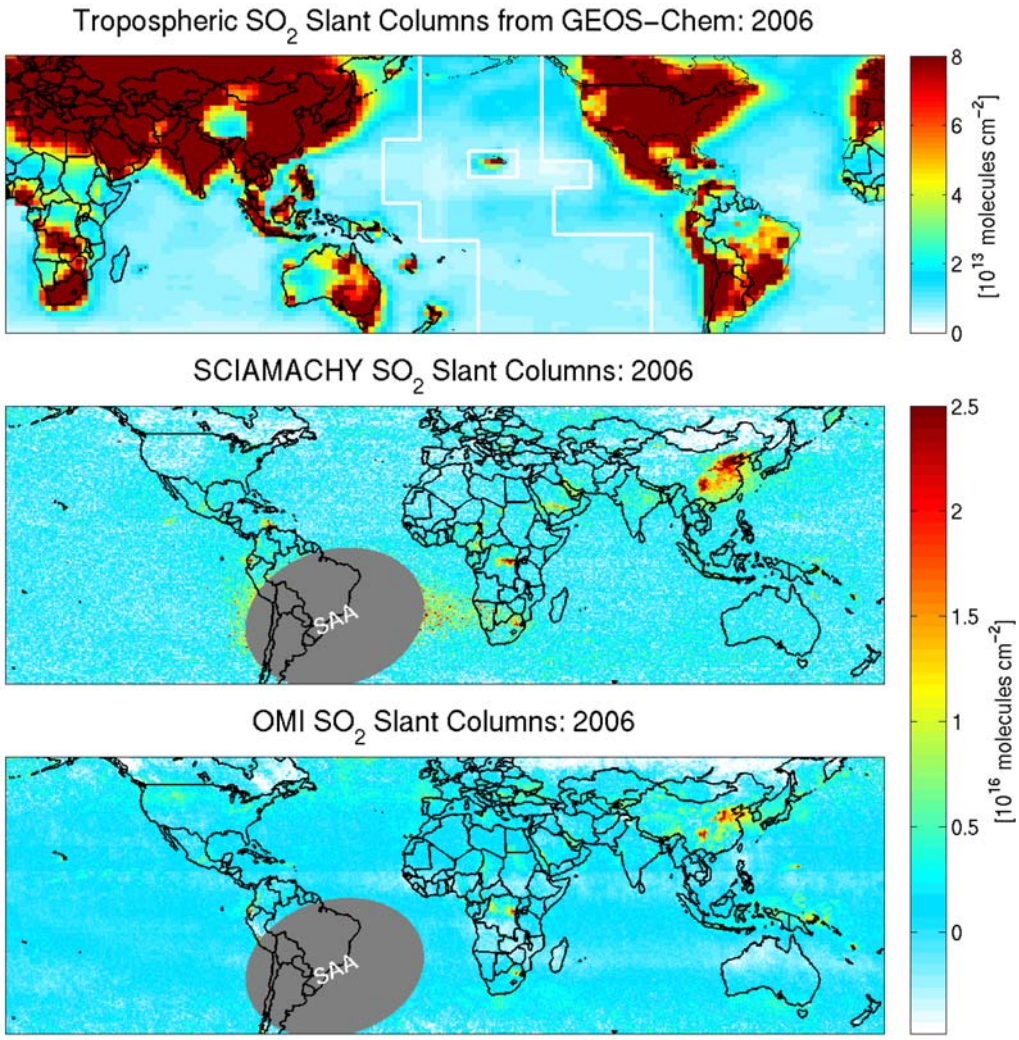

Figure 5. Annual mean tropospheric SO_2 slant columns for 2006. (top) Columns simulated with the GEOS-Chem model. The GEOS-Chem slant columns are obtained from the simulated vertical columns sampled for OMI overpass time using the OMI SO_2 AMF. The white lines denote the reference sector over the central Pacific region that is used for an offset correction to the slant column. Offset-corrected slant columns from (middle) SCIAMACHY and (bottom) OMI.

sensitivity to ozone profile; the assumed a priori ozone profile in step 1 OMTO3 algorithm is switched from a low-latitude shape to a midlatitude shape at ± 30° latitude in the ozone lookup table [*Bhartia and Wellemeyer*, 2002]. Differences with SCIAMACHY arise from the sliding median correction applied to OMI residuals, from differences in spectral fitting, and from instrument differences.

[33] We remove the latitude-dependent offsets in SCIAMACHY and OMI SO_2 slant columns by subtracting the columns taken over the Pacific from the total column on a daily basis using the reference sector method (RSM, following *Martin et al.* [2002] and *Richter and Burrows* [2002] for NO_2 and *Khokhar et al.* [2005] for SO_2). We recognize that the offset may actually depend on the true SO_2 concentration and consider this approach a temporary fix until the offset is addressed in a future improved spectral fit. We use the GEOS-Chem model to identify regions with little SO_2.

[34] Figure 5 (top) shows simulated GEOS-Chem SO_2 slant columns. Much of the Pacific Ocean, excluding volcanic regions such as Hawaii, has little SO_2 (mean simulated values $< 3.0 \times 10^{13}$ molecules cm^{-2}) and is suitable for the offset correction. In situ SO_2 measurements from INTEX-B over the North Pacific confirm the low SO_2 concentrations (Figure 3). The stratosphere also has little SO_2 ($<1 \times 10^{14}$ molecules cm^{-2}) barring exceptional volcanic events [*Inn and Vedder*, 1981; *Pyle et al.*, 1996]. We note that the May 2006 eruption of the Soufriere Hill volcano in Caribbean sent an SO_2 cloud into stratosphere that crossed the Pacific sector at ~20 km height [*Prata et al.*, 2007]. The areas of volcanic plume are excluded from the reference sector for 25 May to 12 June 2006.

[35] Figure 5 (bottom) show the SCIAMACHY and OMI SO_2 slant columns corrected for latitude-dependent offsets using RSM. Their overall consistency is more apparent. Differences between the SCIAMACHY and OMI slant

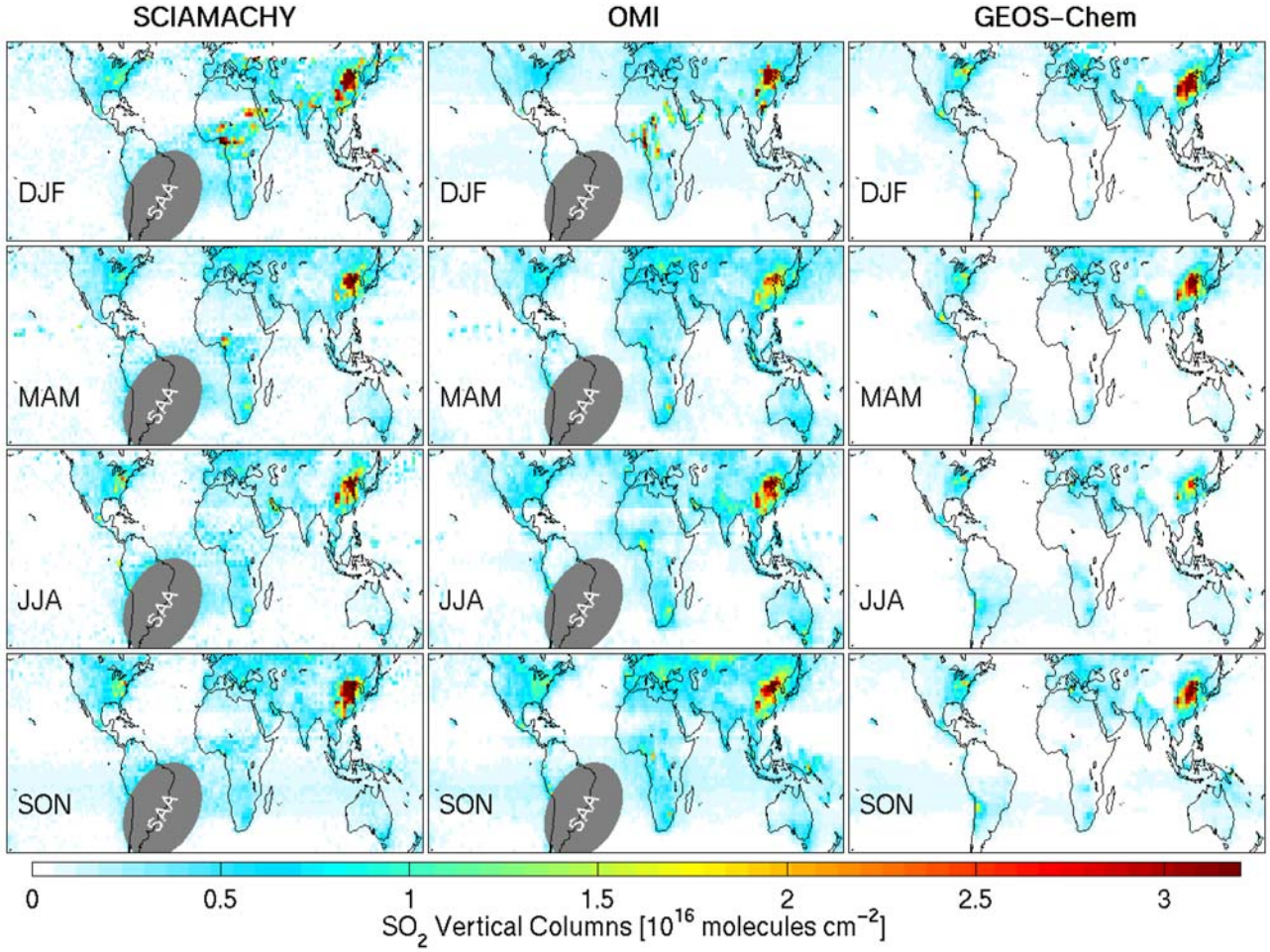

Figure 6. Seasonal mean tropospheric vertical columns of SO_2 for mostly clear scenes (cloud radiance fraction < 0.2).

columns in Figure 5 partially reflect their pixel size and sampling as described in Table 1. Differences in the spectral fit also contribute.

4.2. Vertical Columns

[36] We calculate SO_2 vertical columns from SCIAMACHY and OMI by dividing each slant column with the coincident local AMF determined with the GEOS-Chem simulation for the respective instrument overpass times. Seasonal mean values of the resulting vertical columns regridded onto the GEOS-Chem grid are shown in Figure 6. The spatial distributions of the vertical columns of SCIAMACHY and OMI SO_2 resemble those of their slant columns. However, the AMF conversion from slant to vertical columns generally enhances the columns over land (AMF < 1), and decreases those over oceans and volcanoes (AMF > 1).

[37] Both SCIAMACHY and OMI show enhanced SO_2 columns over metropolitan and industrial areas, especially over eastern China. Both instruments observe volcanic SO_2 plumes from explosive eruptions. The SO_2 plume form the Nyamuragira, Congo is apparent in DJF extending from Central Africa to South Asia. The SO_2 plume from the Soufriere Hills, Caribbean volcano extends over the tropical Pacific in May [*Prata et al.*, 2007].

[38] However, distinct differences exist between SCIAMACHY and OMI. The seasonal variation of SO_2 columns over China reaches a minimum in summer for SCIAMACHY and in spring for OMI. The SCIAMACHY columns tend to be $3-5 \times 10^{15}$ molecules cm^{-2} higher than OMI columns over industrial regions of Western Europe, the eastern United States, and South Asia, and $1-2 \times 10^{16}$ molecules cm^{-2} higher over East China. However, in summer, the OMI columns are $1-2 \times 10^{16}$ molecules cm^{-2} higher over eastern China than those from SCIAMACHY. There is a difference of $1-2 \times 10^{16}$ molecules cm^{-2} between SCIAMACHY and OMI columns over volcanic regions of Central Africa in DJF and Indonesia in the periods of DJF and SON.

4.3. Validation of the SO_2 Retrieval With Airborne in Situ Measurements

[39] Here we use the aircraft measurements from INTEX-A and INTEX-B to evaluate the satellite retrievals. Aircraft spirals are selected for validation if they satisfy the following coincidence criteria: (1) the profile measurement must have been made during daytime within a SCIAMACHY and OMI scene on the date of observation and (2) the in situ measurements must sample the lower troposphere below 0.6 km and up to at least 3 km. The reason for the second

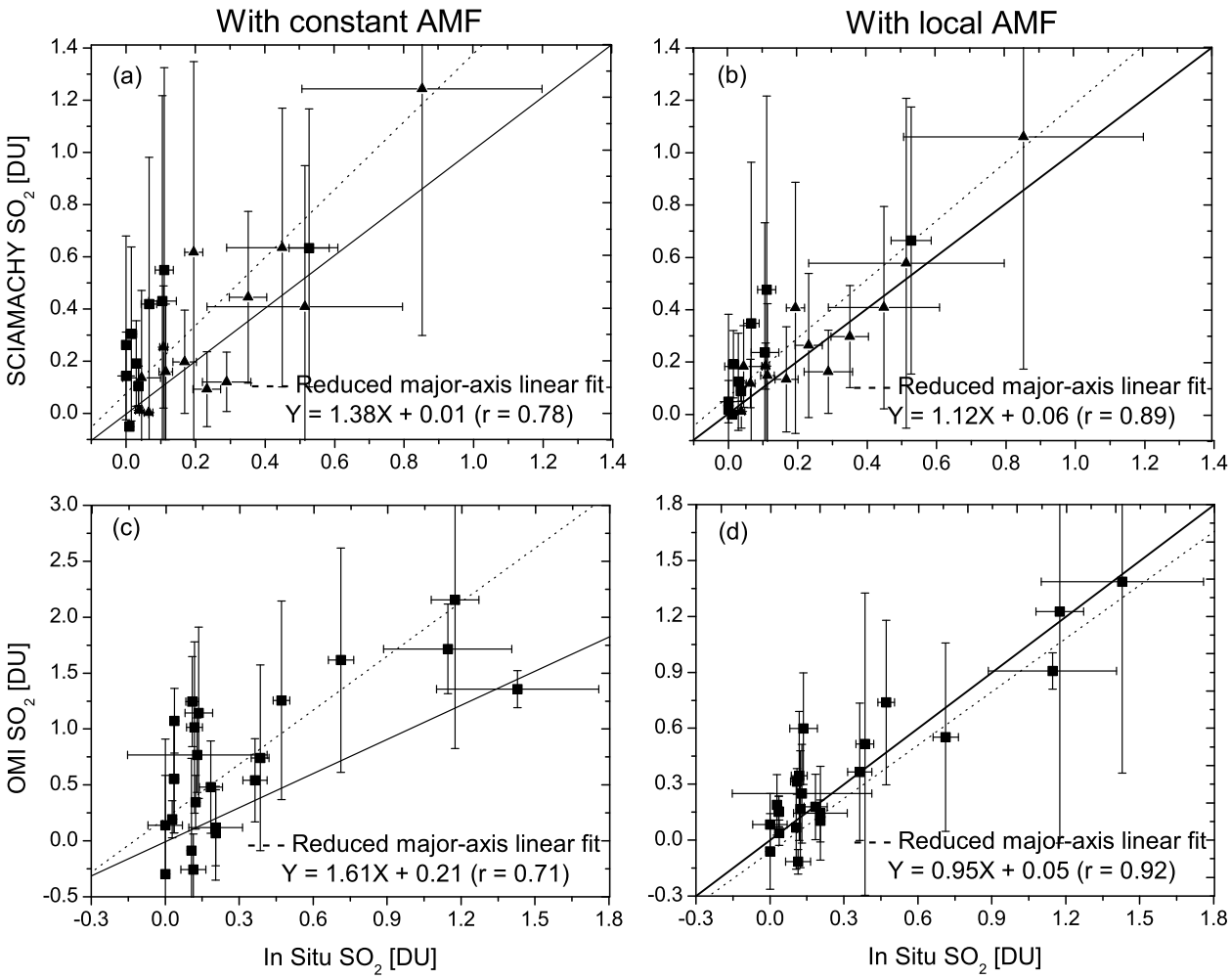

Figure 7. Scatterplots of tropospheric SO_2 vertical columns from (a and b) SCIAMACHY and (c and d) OMI versus those from in situ measurements during INTEX-A (triangles) and INTEX-B (squares). The constant AMF refers to the OMI operational PBL product. The local AMF is developed in this paper. Error bars indicate the standard deviations of in situ measurements and the SCIAMACHY retrieval error. The solid line represents the Y = X line. The dotted lines were calculated with reduced major-axis linear regression [*Hirsch and Gilroy*, 1984].

criterion is that the column is often dominated by boundary layer SO_2. Satellite measurements with pixel centers within 15 km of the aircraft spiral are used for the comparison. Twenty three coincident measurements for INTEX-A and INTEX-B combined are available during SCIAMACHY overpasses, and 23 measurements alone for INTEX-B during OMI overpasses. The locations of coincident measurements are shown in Figure 2.

[40] Partial columns from airborne measurements are calculated by integrating the average SO_2 amount from the lowest to the highest measurement altitude. The partial column below the lowest measurement altitude of an individual profile is obtained by integrating a mean SO_2 amount from the values measured below 1 km, assuming the mixing ratio from the surface to 1 km is homogeneous. This partial column is typically 10–30%. The partial column above the highest measurement altitude of an individual profile is determined by integrating to 12 km a mean profile obtained from all flights over each campaign. This partial column is typically < 3%. These three partial columns are integrated for comparison with column amounts of a collocated satellite measurement pixel.

[41] Figure 7 compares SO_2 vertical columns retrieved from SCIAMACHY (Figures 7a and 7b) and OMI (Figures 7c and 7d) with those determined with airborne in situ measurements for INTEX-A and INTEX-B. Figures 7b and 7d shows the SO_2 columns retrieved using the local AMF are highly consistent with the in situ measurements (correlation coefficient r = 0.89 for SCIAMACHY and r = 0.92 for OMI). The slopes of the reduced major-axis regression lines are 1.12 for SCIAMACHY and 0.95 for OMI. The comparison exhibits moderate scatter that could be related to incomplete in situ sampling of the entire column, diurnal variation of SO_2, and the uncertainty of the measurements.

[42] To further evaluate the local AMF, Figure 7 (left) compares the in situ SO_2 columns from INTEX-A and INTEX-B with the RSM-corrected satellite SO_2 columns that use a globally uniform AMF of 0.88 [*Lee et al.*, 2008a] for SCIAMACHY and of 0.36 for OMI [*Krotkov et al.*,

Table 3. Comparison Over China of SO_2 Columns From Airborne in Situ Measurements and OMI[a]

Statistics	OMI SO_2		
	Local AMF[b]	Operational AMF[c]	Aircraft AMF-Corrected[d]
Correlation Coefficient, r	0.90 (p = 0.002)	0.83 (p = 0.01)	0.92 (p = 0.001)
Slope[e]	0.96	0.97	1.00
Offset[e] (molecules cm^{-2})	8.6×10^{15}	1.6×10^{16}	1.7×10^{16}

[a]Aircraft in situ SO_2 columns (n = 8) in Table 3 of *Krotkov et al.* [2008] measured over China during EAST-AIRE campaign. The aircraft spiral locations are 41°N–43°N, 122°E–234°E.
[b]OMI SO_2 columns calculated in this study.
[c]Collection 3 OMI SO_2 columns in Table 3 of *Krotkov et al.* [2008] using the operational AMF of 0.36.
[d]Collection 3 OMI SO_2 columns in Table 3 of *Krotkov et al.* [2008] in which the aircraft-measured SO_2 and aerosol profiles, total ozone, and OMI viewing geometry are used in the AMF calculation.
[e]The slope and offset are determined with reduced major-axis linear regression [*Hirsch and Gilroy*, 1984].

2008]. Correlations of the aircraft and retrieved columns are reduced (r = 0.78 for SCIAMACHY and r = 0.71 for OMI) when a globally uniform AMF is used. Evaluation of the other OMI SO_2 products (lower tropospheric and midtropospheric algorithms) with aircraft observations yielded worse results (r < 0.59).

[43] We also compare SO_2 columns from in situ aircraft measurements over eastern China [*Krotkov et al.*, 2008] with those retrieved from OMI. Table 3 contains the statistics for the comparison. Replacing the global uniform AMF of 0.36 with our local AMF improves the correlation from 0.83 to 0.90, and reduces the offset by a factor of 2. The consistency of the aircraft SO_2 columns with the retrieved using our local AMF is comparable to the performance when the aircraft measurements themselves are used for the AMF correction, providing further confidence in our AMF calculation.

4.4. Comparison to Atmospheric Chemistry Model

[44] Figure 6 (right) shows seasonal mean simulated GEOS-Chem SO_2 columns for 2006, sampled coincidently with SCIAMACHY observations. Sampling GEOS-Chem during OMI observations changes seasonal mean values by less than 4×10^{15} molecules cm^{-2}. The global distribution of the GEOS-Chem columns is generally consistent with the observed columns from SCIAMACHY (r = 0.79, slope = 1.59, offset = 1×10^{15} molecules cm^{-2}) and OMI (r = 0.77, slope = 0.89, offset = 2×10^{15} molecules cm^{-2}). The AMF had a minor effect on the correlation. The correlation of GEOS-Chem slant columns with satellite slant columns is 0.76 for SCIAMACHY and 0.71 for OMI. Simulated and retrieved vertical columns both exhibit clear enhancements over China. The most pronounced disagreements are found for explosive volcanic eruption regions (e.g., Central Africa in DJF from the Nyamuragira and the topical Pacific in MAM from the Soufriere Hills volcano).

[45] Table 4 presents a more focused comparison over the United States, where bottom-up SO_2 emission inventories are expected to be well known. The seasonal mean SO_2 columns from SCIAMACHY and OMI are spatially well correlated with those determined from the GEOS-Chem model (r = ~0.85 for SCIAMACHY and r = ~0.82 for OMI). However, the SCIAMACHY SO_2 columns are 4×10^{15} molecules cm^{-2} (30–70%) higher than the corresponding values from the GEOS-Chem model, with the largest differences in summer. The OMI observations are typically 10–50% ($2–5 \times 10^{15}$ molecules cm^{-2}) lower over the eastern United States than the corresponding values from the GEOS-Chem model, with the largest differences in spring. The correlation of GEOS-Chem slant columns with satellite slant columns is within 0.04 of the correlations reported for vertical columns in Table 4.

[46] Table 4 also compares simulated and retrieved values over eastern China, where bottom-up inventories are less well known than for the United States. Observations from SCIAMACHY and OMI again are well correlated with those from the GEOS-Chem (r = ~0.85 for SCIAMACHY and r = ~0.81 for OMI). However, the SCIAMACHY columns are 20–60% higher than those from GEOS-Chem in winter, spring and fall and 50–120% higher in summer. The OMI columns are 40% lower than those from GEOS-Chem in fall through spring, and 60% higher in summer.

[47] Several pronounced differences are found elsewhere in the world. The SO_2 columns from SCIAMACHY and OMI are a factor of 2–3 higher than those from GEOS-Chem over Nigeria and over the Highveld of South Africa, a

Table 4. Comparison of Seasonal Mean Simulated and Retrieved SO_2 Vertical Columns for 2006[a]

Period	United States[b]		Eastern China[c]	
	SCIAMACHY (molecules cm^{-2})	OMI (molecules cm^{-2})	SCIAMACHY (molecules cm^{-2})	OMI (molecules cm^{-2})
Winter (DJF)	$1.28 \times GC - 1.43 \times 10^{14}$ (r = 0.90, p < 0.001)	$0.73 \times GC - 3.04 \times 10^{14}$ (r = 0.87, p < 0.001)	$1.39 \times GC - 4.23 \times 10^{15}$ (r = 0.75, p < 0.001)	$0.94 \times GC - 4.79 \times 10^{15}$ (r = 0.65, p < 0.001)
Spring (MAM)	$1.31 \times GC - 4.79 \times 10^{14}$ (r = 0.84, p < 0.001)	$0.87 \times GC - 3.59 \times 10^{14}$ (r = 0.82, p < 0.001)	$1.19 \times GC - 1.33 \times 10^{15}$ (r = 0.89, p < 0.001)	$0.61 \times GC - 1.02 \times 10^{15}$ (r = 0.83, p < 0.001)
Summer (JJA)	$1.73 \times GC - 5.05 \times 10^{15}$ (r = 0.83, p < 0.001)	$1.17 \times GC - 4.04 \times 10^{14}$ (r = 0.79, p < 0.001)	$2.37 \times GC - 1.69 \times 10^{15}$ (r = 0.88, p < 0.001)	$1.58 \times GC - 6.63 \times 10^{14}$ (r = 0.92, p < 0.001)
Fall (SON)	$1.54 \times GC - 5.88 \times 10^{14}$ (r = 0.85, p < 0.001)	$0.97 \times GC - 4.62 \times 10^{14}$ (r = 0.82, p < 0.001)	$1.67 \times GC - 1.91 \times 10^{15}$ (r = 0.89, p < 0.001)	$0.78 \times GC - 1.29 \times 10^{15}$ (r = 0.85, p < 0.001)

[a]Equations are determined with reduced major-axis linear regression [*Hirsch and Gilroy*, 1984]. The GEOS-Chem simulation is sampled coincidently with the instrument being compared. GC denotes GEOS-Chem.
[b]25°N–50N°, 127°W–68°W; 336 cases.
[c]25°N–45°N, 100°E–125°E; 153 cases.

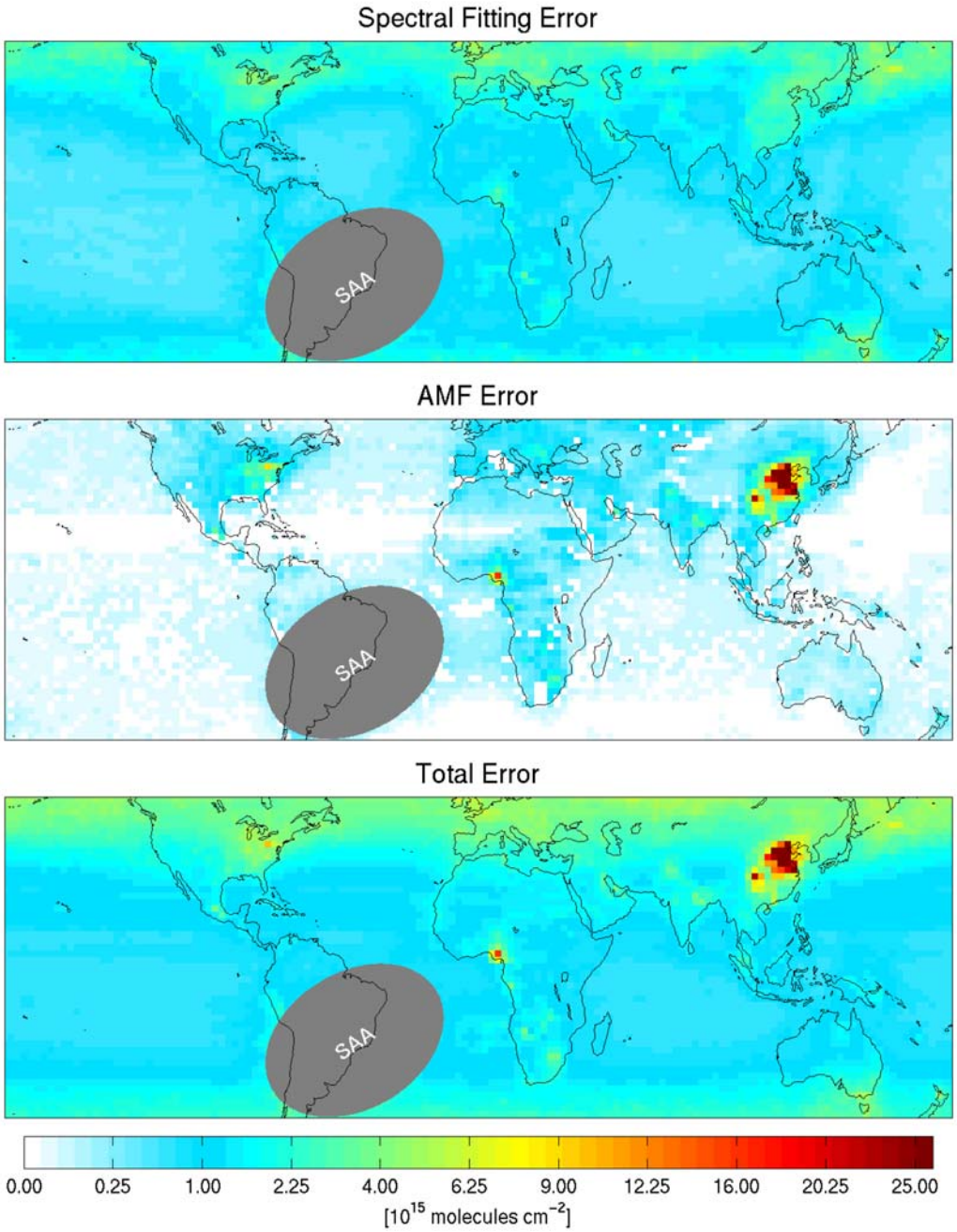

Figure 8. Annual mean errors in the SO_2 retrieval from SCIAMACHY for mostly clear scenes (cloud radiance fraction < 20%). The (bottom) total errors are calculated as the quadrature sum (equation (10)) of the (top) spectral fitting errors, (middle) AMF errors, and errors in removal of the slant column bias.

region with numerous power plants. Retrieved values are 20–80% higher than simulated values around the Persian Gulf, industrial regions of Europe, Indonesian volcanic regions and southeastern Australia. Retrieved values are 50–70% lower than simulated over the Himalaya region and Mexico. There are also large differences over volcanic regions as noted earlier.

5. Error Analysis of SO_2 Retrieval

[48] The main errors of satellite measurements of SO_2 columns come from uncertainties of spectral fitting, removal of the slant column bias, and the AMF calculation. Here we quantify the errors.

5.1. Errors in Slant Columns

[49] Figure 8 (top) shows the annual mean errors from spectral fitting in the retrieval of SO_2 vertical columns from SCIAMACHY. We use the SCIAMACHY fitting errors here since they are available for each individual observation. The annual mean slant column errors from spectral fitting are calculated by Gaussian error propagation of the individual errors, normalized by their corresponding AMFs

for comparison with vertical column errors. The resulting error is $\sim 3.5 \times 10^{15}$ molecules cm^{-2} (20%) over polluted areas at the GEOS-Chem resolution of $2° \times 2.5°$. The error in daily OMI slant columns over polluted areas at the GEOS-Chem resolution is $\sim 6 \times 10^{15}$ molecules cm^{-2} (<45%) [*Krotkov et al.*, 2008]. The slant column error is associated with an imperfect spectral fit reflecting spectral interference and weak radiances measured at UV wavelengths. Absolute errors are higher over polluted regions where SO_2 columns are larger, and at high latitudes where enhanced ozone columns reduce fitting precision. Annual mean slant column errors are smaller than signals from major anthropogenic SO_2 sources.

[50] We estimate the error in the offset removal (section 4.1), as the quadrature sum of the annual mean slant column error over the reference sector and the difference between simulated and INTEX-B aircraft SO_2 columns over the Pacific. The corresponding error is $< 0.4 \times 10^{15}$ molecules cm^{-2} in the tropics and $0.4–1.2 \times 10^{15}$ molecules cm^{-2} at higher latitudes.

5.2. Errors of the Air Mass Factor

[51] The error in the AMF calculation depends on surface reflectivity, clouds, aerosols, and the SO_2 vertical profile [*Khokhar et al.*, 2005; *Krotkov et al.*, 2008; *Richter et al.*, 2006]. We assess the local error from surface reflectivity by comparing AMFs recalculated using the surface reflectivity uniformly perturbed by its uncertainty of 0.02 [*Herman and Celarier*, 1997; *Boersma et al.*, 2004; *Millet et al.*, 2006]. We determine the local error from cloud pressure by perturbation with its uncertainty of 100 hPa [*Vasilkov et al.*, 2008; *P. Wang et al.*, 2008]. The spatial variation in the uncertainty in the SO_2 profile is difficult to assess because of a paucity of measured SO_2 profiles. The campaign mean comparisons presented in section 3.2 of AMFs calculated with either aircraft-measured or simulated SO_2 shape factors found differences of 10%, with no clear spatial variation. We refer to this error as the profile bias. We estimate the local daily error from the shape factor as half of the difference in AMFs with a monthly mean local SO_2 profile versus a daily local SO_2 profile. We add in quadrature the daily shape factor errors and profile bias. The error due to aerosols depends on a variety of aerosol parameters: the size distribution, refractive index, shape, and vertical distribution. Due to the large uncertainty in UV aerosol absorption we assume a 50% error on the aerosol correction. Error from ozone is estimated using the uncertainty in the O_3 column retrieval of 5% [*Weber et al.*, 2007]. We assess error from wavelength dependence by comparing AMFs calculated at three wavelengths for peaks of the SO_2 absorption cross section nearest to the middle and edges of the fitting window.

[52] Figure 9 shows the resulting daily, local errors from surface reflectivity, cloud pressure, SO_2 profile, and aerosols for SCIAMACHY measurements for 2006. The left column contains errors for the clear-sky AMF calculation. The right column contains errors for the completely cloudy AMF subpixel calculation. The error due to surface reflectivity ranges from 8 to 15% over land and <8% over ocean. The sensitivity of the AMF to surface reflectivity is roughly twice as large for polluted situations as for unpolluted situations, and is generally larger for smaller surface reflectivity. Surface reflectivity is irrelevant for opaque clouds as treated here for consistency with the FRESCO+ and OMICLDRR cloud products. The error due to cloud pressure ranges from <10% over ocean to >100% over land. Clouds enhance the instrument sensitivity to SO_2 above the cloud, and decrease the instrument sensitivity to SO_2 below cloud. The sensitivity of the AMF to cloud pressure is high when the cloud is collocated with high SO_2 mixing ratios, such as over China. Cloud pressure generally has little effect on the AMF over pristine regions. The error due to SO_2 profile uncertainty is generally 10–22% for clear sky AMF. The errors are higher (20–120%) for the cloudy sky AMF reflecting increased profile sensitivity in the presence of cloud. Larger errors at high latitudes reflect high variability in the SO_2 profile and larger light paths. The estimated error from aerosols is highest over polluted regions (i.e., eastern China) and dusty regions (i.e., the Sahara). Error from UV-absorbing aerosols increases in the presence of clouds due to multiple scattering. Error from ozone is generally <1%. Error from wavelength dependence of the AMF is generally 6–14% in both clear and cloudy-sky AMF. Figure 9 shows the error in the clear-sky (Figure 9g) and cloudy-sky (Figure 9h) AMF expressed as the quadrature sum of errors due to uncertainties of surface reflectivity, cloud pressure, shape factor, aerosols, ozone, and wavelength. The clear-sky AMF error ranges from 15 to 30% over land and <15% over ocean. The cloudy-sky AMF error is 80–160% over polluted regions and less elsewhere.

[53] We estimate the AMF error ε_{AMF} for each measurement using AMF_{clear} and AMF_{cloud}, and their errors, $\varepsilon_{AMFclear}$ and $\varepsilon_{AMFcloud}$ following *Wenig et al.* [2008],

$$\varepsilon_{AMF} = \sqrt{(\mathrm{AMF}_{cloud} - \mathrm{AMF}_{clear})^2 \varepsilon_c^2 + c^2 (\varepsilon_{AMFcloud})^2 + (1-c)^2 (\varepsilon_{AMFclear})^2}. \quad (8)$$

The error of the cloudy radiance fraction ε_c follows *Wenig et al.* [2008]

$$\varepsilon_c = \sqrt{\left(\left(\frac{c \cdot (1-f)^2 \cdot \varepsilon_{SR}}{(1-c) \cdot R_{cloud}}\right)^2 + \varepsilon_f^2\right)^2 \cdot \left(\frac{c \cdot (1-c)}{f \cdot (1-f)}\right)^2}. \quad (9)$$

We assume an error in the cloud fraction $\varepsilon_f = 0.1$ on the low side [*Vasilkov et al.*, 2008; *P. Wang et al.*, 2008] and an error in the surface reflectivity $\varepsilon_{SR} = 0.02$ [*Herman and Celarier*, 1997; *Boersma et al.*, 2004].

[54] Figure 10 shows the AMF error for each observation as a function of effective cloud fraction. The AMF error for unpolluted scenes ranges from 12% for cloud-free conditions to 53% for completely cloudy scenes. However, for polluted scenes it rapidly increases from 21% for cloud-free conditions to 245% for completely cloudy, reflecting the error in the correction for SO_2 obscuration by clouds.

[55] Figure 8 (middle) shows the global distribution of the daily AMF error for SCIAMACHY measurements of mostly clear scenes (cloud radiance fraction < 20%). In construction of the annual mean errors, we take the errors in cloud pressure and the daily SO_2 profile to be random. Errors in surface reflectivity, aerosols, and the SO_2 profile

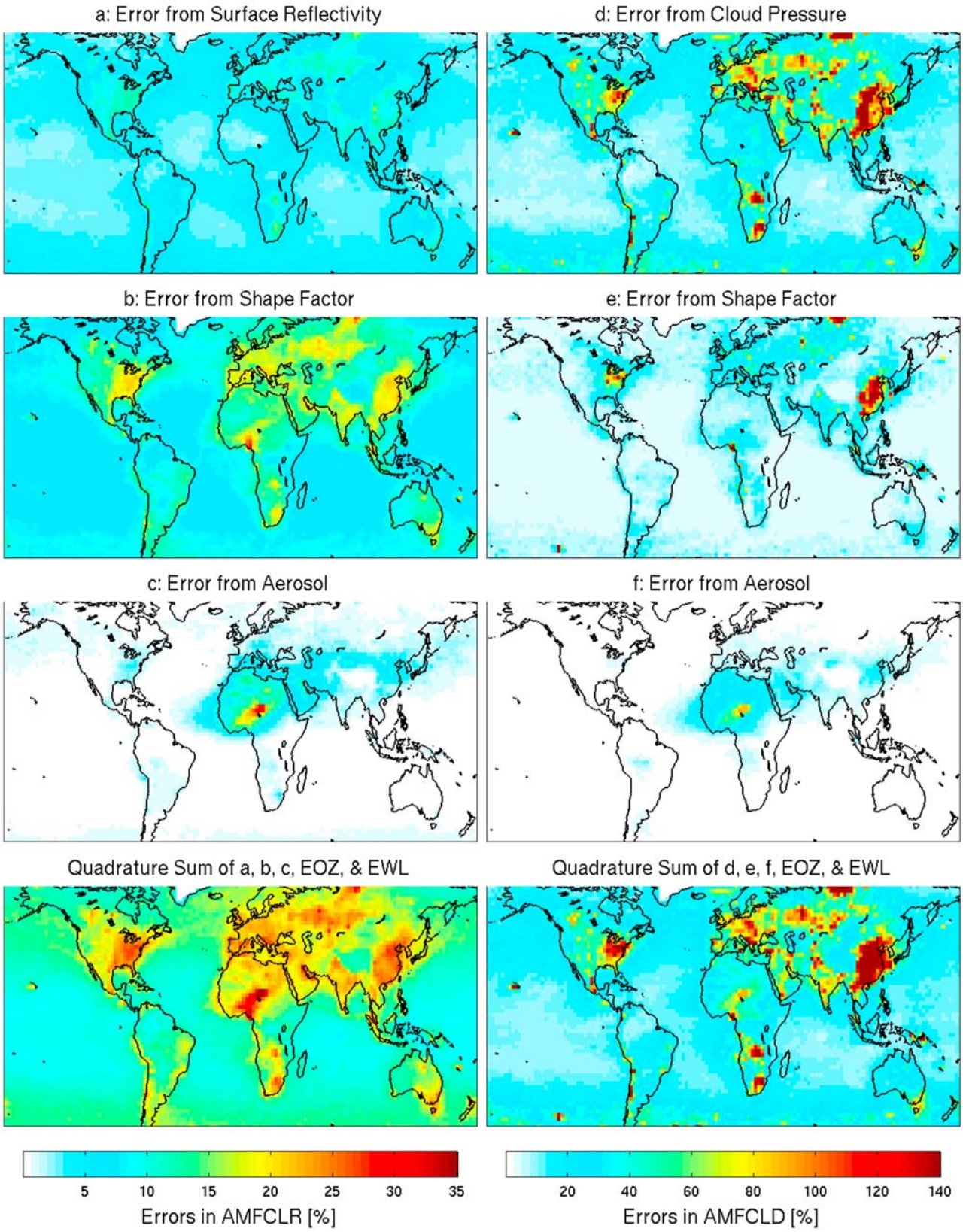

Figure 9. Local errors for individual observations due to uncertainties of (a) surface reflectivity, (d) cloud pressure, (b and e) SO_2 profile, and (c and f) aerosols in the AMF calculation for SCIAMACHY measurements. (left) The errors in the clear-sky AMF (AMFCLR). (right) The errors in the cloudy-sky AMF (AMFCLD). Quadrature sum of surface reflectivity, cloud pressure, SO_2 profile, aerosols, ozone (EOZ), and wavelength (EWL), separately for (g) clear and (h) cloudy subpixels.

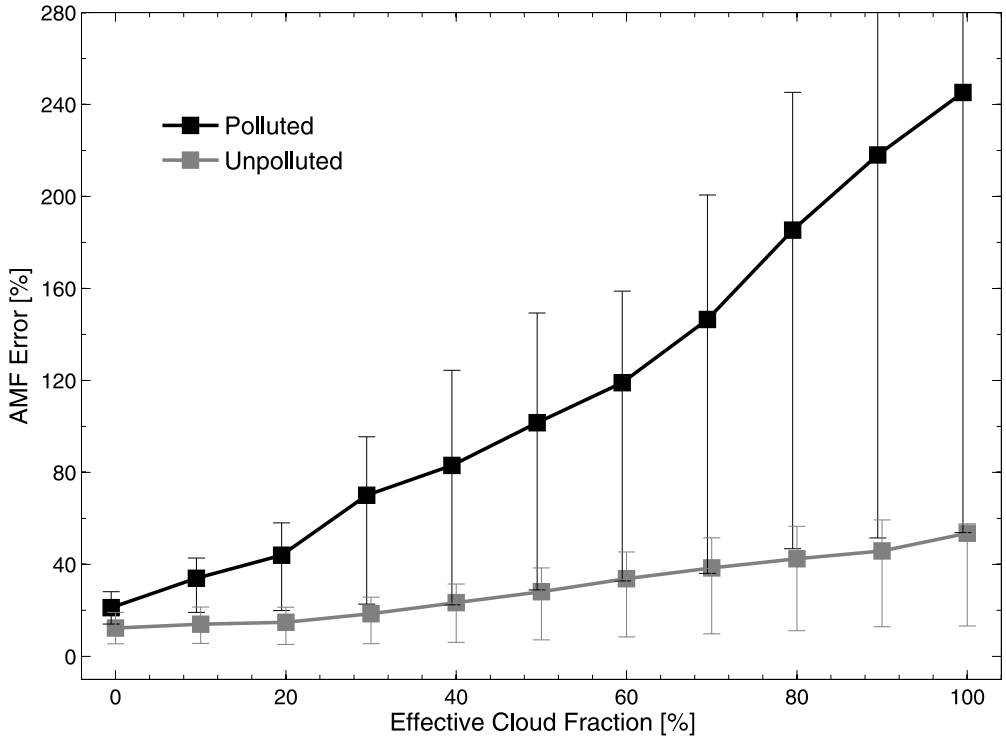

Figure 10. Mean global AMF error for individual observations as a function of cloud fraction. The AMF error is calculated using equation (8) for polluted ($\geq 1.0 \times 10^{16}$ molecules cm^{-2}) and unpolluted cases ($<1.0 \times 10^{16}$ molecules cm^{-2}) from SCIAMACHY measurements for 2006. Error bars represent the 17th and 83rd percentiles.

bias are taken to be systematic. AMF errors are $<2 \times 10^{15}$ molecules cm^{-2} for most of the world. Enhanced AMF errors are found in polluted areas such as the eastern United States where the SO_2 errors due to AMF range from 3 to 5×10^{15} molecules cm^{-2} (35–50%) and China where errors are up to 2.2×10^{16} molecules cm^{-2} (70%). The enhanced AMF error over Nigeria arises from particularly large uncertainty in the aerosol correction over strong SO_2 sources (Figure 9c). AMF errors in the OMI measurements are generally within 15% of those in the SCIAMACHY measurements.

5.3. Total Error in the SO_2 Retrievals

[56] We express the total error ε in the retrieval of vertical SO_2 columns as follows:

$$\varepsilon = \sqrt{\left(\frac{\varepsilon_{SC}}{\mathrm{AMF}}\right)^2 + \left(\frac{\varepsilon_{RSM}}{\mathrm{AMF}}\right)^2 + \left(\frac{\varepsilon_{AMF}}{\mathrm{AMF}} \cdot VC\right)^2}, \qquad (10)$$

where ε_{SC} and ε_{RSM} are the errors in slant column fitting and removal of the slant column bias, respectively. The normalization by AMF is for comparison of vertical column errors. Figure 8 (bottom) shows the total error. It is dominated by the AMF error over polluted areas, and by the spectral fit elsewhere. The overall error ranges from 3×10^{15} to 7×10^{15} molecules cm^{-2} (40–55% relative errors) for yearly averages over the eastern United States, and up to 2.6×10^{16} molecules cm^{-2} (80% relative errors) for China. Overall errors in the OMI retrieval are within 8% of those in the SCIAMACHY retrieval, assuming the OMI slant column error is consistent with the SCIAMACHY slant column error.

6. Sensitivity of Retrieved SO_2 Columns to Emissions

[57] Of interest is the ability of satellite retrievals of SO_2 to discern information about anthropogenic SO_2 emissions. We examine this question by conducting a sensitivity simulation with GEOS-Chem in which the anthropogenic SO_2 emissions for 2006 are replaced with those for 1998. Emissions from North America increase by a factor of 1.7, and from Europe by a factor of 2.2. Emissions from China decrease by a factor of 2.1. The meteorology of the simulation remains specific to the year 2006.

[58] Figure 11 (top) shows the difference between annual mean SO_2 columns calculated with GEOS-Chem using emissions for 2006 minus one with emissions for 1998. Pronounced differences of a factor of 2 are found over the regions with large changes in emissions, in particular over North America, Europe, and China. We compare this change in SO_2 columns to the retrieval bias that would arise from using incorrect SO_2 shape factors. Figure 11 (bottom) shows the difference between annual mean OMI SO_2 columns for 2006 retrieved using SO_2 shape factors from the simulation with 2006 emissions, minus the one using SO_2 shape factors from simulation with 1998 emissions. The retrieved SO_2 columns using shape factors for 1998 emissions are within 30% of those retrieved using shape factors for 2006 emissions. The larger changes in SO_2 columns of the reference atmosphere, compared with the

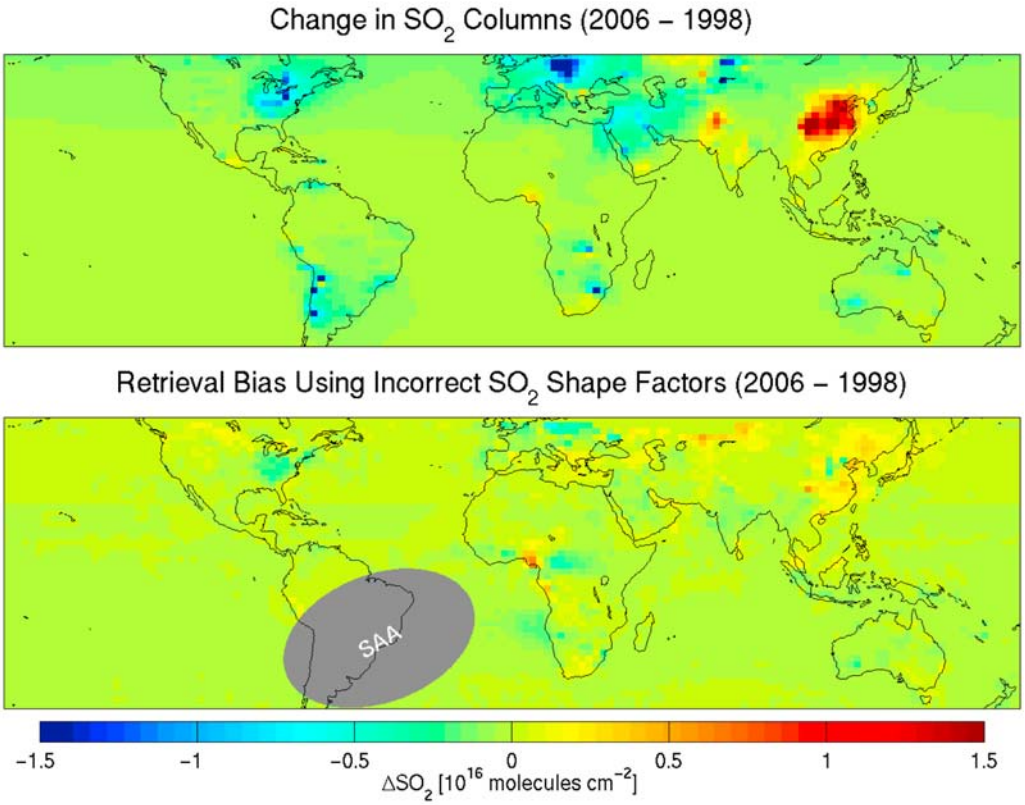

Figure 11. Sensitivity of SO_2 columns to errors in anthropogenic emissions. (top) The difference between GEOS-Chem simulations of SO_2 columns using meteorology for 2006 with anthropogenic emissions for 2006 minus one with emissions for 1998. (bottom) The difference between OMI SO_2 columns for 2006 retrieved using SO_2 shape factors from the GEOS-Chem simulations with anthropogenic SO_2 emissions for either 2006 or 1998.

smaller retrieval bias from incorrect SO_2 shape factors, indicate a clear sensitivity of SCIAMACHY and OMI to anthropogenic SO_2 emissions.

7. Conclusion

[59] Sulfur dioxide (SO_2) is released by natural and anthropogenic processes into the Earth's atmosphere where it plays important roles in climate and ecosystem health. We have presented an improved retrieval of SO_2 vertical columns from the SCIAMACHY and OMI satellite instruments. Attention was devoted to the development of an air mass factor (AMF) algorithm to convert slant columns to vertical columns. For each observation from SCIAMACHY and OMI, we calculated an AMF from the altitude-dependent scattering weights computed with a radiative transfer model (LIDORT), weighted by relative vertical SO_2 distribution (shape factor) determined locally with a 3-D global model of atmospheric chemistry (GEOS-Chem). The AMF calculation uses a 14 year local surface reflectivity climatology determined from TOMS at 360 nm. Cloud scattering is accounted for using cloud fraction and cloud pressure determined with the FRESCO+ algorithm for SCIAMACHY or the OMCLDRR algorithm for OMI. We accounted for the effect of ozone (O_3) absorption on the AMF by using O_3 columns retrieved from SCIAMACHY and OMI. Scattering and absorption of radiation by aerosols is accounted for using simulated vertically resolved aerosol optical properties.

[60] The AMF calculation reveals a factor of four variation in the seasonal mean sensitivity of SCIAMACHY and OMI to SO_2. In general, both instruments are about twice as sensitive to SO_2 columns over ocean than over land, because atmospheric scattering reduces instrument sensitivity to SO_2 at low altitudes, and the center of mass SO_2 pressure is lower over oceans than over land. Absorption of ultraviolet radiation by mineral dust can decrease the instrument sensitivity by 10–50% over deserts and downwind regions affected by dust transport (e.g., northeastern China in spring).

[61] Latitudinally dependent offsets in SCIAMACHY and OMI slant columns were diagnosed by comparing retrieved, simulated, and aircraft columns over the Pacific. The offsets were removed by subtracting zonal mean values through the reference sector method. We evaluated the GEOS-Chem SO_2 shape factors with airborne in situ measurements from the INTEX-A and INTEX-B aircraft campaigns over the North Pacific, North America, and the North Atlantic. Differences between simulated and retrieved profiles would change the AMF by 10%.

[62] We validated the retrieved SO_2 columns from SCIAMACHY and OMI with coincident in situ measurements from INTEX-A and INTEX-B. Application of the local AMFs calculated here improved the consistency of the

aircraft measurements versus the SCIAMACHY retrievals (correlation increases from 0.78 to 0.89; slope decreases from 1.38 to 1.12) and versus the OMI retrievals (correlation increases from 0.71 to 0.92; slope decrease from 1.61 to 0.95). Validation of the retrieved OMI SO_2 columns versus aircraft measurements over eastern China yields similar improvements: application of our local AMFs increases the correlation from 0.83 to 0.90.

[63] Retrieved SCIAMACHY and OMI vertical columns for 2006 exhibit broad consistency with simulated columns from GEOS-Chem. Over the United States, where SO_2 emissions are particularly well known, seasonal mean simulated and retrieved columns are spatially well correlated (r = 0.85 for SCIAMACHY and r = 0.82 for OMI). The slope of the reduced major axis regression line is 1.47 for SCIAMACHY and 0.93 for OMI. Retrieved columns over eastern China also are highly correlated (r = 0.85 for SCIAMACHY and r = 0.81 for OMI) with those from the GEOS-Chem simulation. However, seasonal mean simulated SO_2 columns over eastern China in winter, spring and fall are 20–60% lower than those from SCIAMACHY and 10–40% higher than those from OMI. In summer the seasonal mean simulated SO_2 columns are 50–120% lower than those from SCIAMACHY and 60% lower than those from OMI.

[64] We conducted sensitivity calculations to estimate the local error in the SO_2 retrieval. The retrieval error is dominated by the spectral fitting precision over remote regions. Over regions of enhanced SO_2 columns ($>1 \times 10^{16}$ molecules cm^{-2}) the AMF calculation becomes a more important contributor to the total error mostly due to uncertainty in clouds, SO_2 vertical profiles, surface albedo, and aerosols. For individual scenes, cloud pressure is the dominant term in the AMF error despite excluding those with cloud radiance fraction > 0.2. After accounting for random errors, the largest contributor to the annual mean AMF error is the SO_2 shape factor.

[65] We examined the sensitivity of SCIAMACHY and OMI to anthropogenic emissions by conducting a sensitivity simulation using emissions for 1998 instead of 2006. Simulated SO_2 columns changed by a factor of 2. However, the SO_2 AMFs changed by less than 30% due to changes in the shape factors. The large difference between the change in AMF and change in simulated SO_2 columns indicates a high sensitivity of SO_2 retrievals to errors in anthropogenic emission inventories.

[66] This study demonstrates that a local AMF calculation is necessary to quantitatively interpret SO_2 observations from solar backscatter instruments such as SCIAMACHY and OMI. A major issue to be resolved is the latitudinally dependent offset in the SCIAMACHY and OMI retrievals, and differences between the retrievals for the two instruments. Better representations of SO_2 oxidation in ship plumes is needed for global models. The SO_2 emissions database of the Global Volcanism Program does not fully capture volcanic emissions. More accurate estimates of volcanic SO_2, ash emissions, and plume heights for each volcanic eruption would improve the global SO_2 simulation and AMF calculation. Direct measurements of aerosol optical properties in the ultraviolet would reduce uncertainty in the AMF.

[67] **Acknowledgments.** We thank Mian Chin for helpful comments on SO_2 emissions. The publicly released planetary boundary layer (PBL) OMI SO_2 Level 2 VC products and OMCLDRR cloud products from OMI were obtained from GES Data and Information Service Center (http://disc.sci.gsfc.nasa.gov/). SO_2 slant columns and WFDOAS total O_3 columns from SCIAMACHY were obtained from the Institute of Environmental Physics and Remote Sensing, University of Bremen, Germany (http://www.iup.uni-bremen.de/). FRESCO+ cloud products from SCIAMACHY were obtained from Tropospheric Emission Monitoring Internet Service (TEMIS) (http://www.temis.nl/). This work was supported by the Natural Science and Engineering Research Council of Canada (NSERC) and by the National Aeronautics and Space Administration (NASA). N. Krotkov acknowledges NASA support through ROSES05 grant NNG06GI00G.

References

Afe, O. T., A. Richter, B. Sierk, F. Wittrock, and J. P. Burrows (2004), BrO emission from volcanoes: A survey using GOME and SCIAMACHY measurements, *Geophys. Res. Lett.*, *31*, L24113, doi:10.1029/2004GL020994.

Alexander, B., J. Savarino, C. C. W. Lee, R. J. Park, D. J. Jacob, M. H. Thiemens, Q. B. Li, and R. M. Yantosca (2005), Sulfate formation in sea-salt aerosols: Constraints from oxygen isotopes, *J. Geophys. Res.*, *110*, D10307, doi:10.1029/2004JD005659.

Andres, R. J., and A. D. Kasgnoc (1998), A time-averaged inventory of subaerial volcanic sulfur emissions, *J. Geophys. Res.*, *103*(D19), 25,251–25,261, doi:10.1029/98JD02091.

Barnard, J. C., R. Volkamer, and E. I. Kassianov (2008), Estimation of the mass absorption cross section of the organic carbon component of aerosols in the Mexico City Metropolitan Area (MCMA), *Atmos. Chem. Phys.*, *8*, 6665–6679.

Beirle, S., U. Platt, R. Von Glasow, M. Wenig, and T. Wagner (2004), Estimate of nitrogen oxide emissions from shipping by satellite remote sensing, *Geophys. Res. Lett.*, *31*, L18102, doi:10.1029/2004GL020312.

Bey, I., D. J. Jacob, R. M. Yantosca, J. A. Logan, B. D. Field, A. M. Fiore, Q. Li, H. Y. Liu, L. J. Mickley, and M. G. Schultz (2001), Global modeling of tropospheric chemistry with assimilated meteorology: Model description and evaluation, *J. Geophys. Res.*, *106*(D19), 23,073–23,095, doi:10.1029/2001JD000807.

Bhartia, P. K., and C. W. Wellemeyer (2002), TOMS-V8 total O_3 algorithm, version 2.0, *ATBD-OMI-02*, NASA Goddard Space Flight Cent., Greenbelt, Md. (Available at http://eospso.gsfc.nasa.gov/eos_homepage/for_scientists/atbd/docs/OMI/ATBD-OMI-02.pdf).

Boersma, K. F., H. J. Eskes, and E. J. Brinksma (2004), Error analysis for tropospheric NO_2 retrieval from space, *J. Geophys. Res.*, *109*, D04311, doi:10.1029/2003JD003962.

Bogumil, K., et al. (2003), Measurements of molecular absorption spectra with the SCIAMACHY Pre-Flight Model: Instrument characterization and reference data for atmospheric remote sensing in the 230-2380 nm region, *J. Photochem. Photobiol. A*, *157*, 167–184.

Carn, S. A., N. A. Krotkov, M. A. Gray, and A. J. Krueger (2004), Fire at Iraqi sulfur plant emits SO_2 clouds detected by Earth probe TOMS, *Geophys. Res. Lett.*, *31*, L19105, doi:10.1029/2004GL020719.

Carn, S. A., A. J. Krueger, N. A. Krotkov, K. Yang, and P. F. Levelt (2007), Sulfur dioxide emissions from Peruvian copper smelters detected by the Ozone Monitoring Instrument, *Geophys. Res. Lett.*, *34*, L09801, doi:10.1029/2006GL029020.

Chance, K. (2005), Ultraviolet and visible spectroscopy and spaceborne remote sensing of the Earth's atmosphere, *C. R. Phys.*, *6*, 836–847.

Chin, M., and D. J. Jacob (1996), Anthropogenic and natural contributions to tropospheric sulfate: A global model analysis, *J. Geophys. Res.*, *101*(D13), 18,691–18,699.

Climate Change Science Program (CCSP) (2009), Atmospheric aerosol properties and climate impacts, report, NASA, Washington, D. C.

Colarco, P. R., O. B. Toon, O. Torres, and F. J. Rasch (2002), Determining the UV imaginary part of refractive index of Saharan dust particles from TOMS data and a three dimensional model of dust transport, *J. Geophys. Res.*, *107*(D16), 4289, doi:10.1029/2001JD000903.

Corr, C. A., N. Krotkov, S. Madronich, J. R. Slusser, B. Holben, W. Gao, J. Flynn, B. Lefer, and S. M. Kreidenweis (2009), Retrieval of aerosol single scattering albedo at ultraviolet wavelengths at the T1 site during MILAGRO, *Atmos. Chem. Phys.*, *9*, 5813–5827.

de Rooij, W. A., and C. C. A. H. van der Stap (1984), Expansion of Mie scattering matrics in generalized spherical functions, *Astron. Astrophys.*, *131*, 237–248.

Dickerson, R. R., et al. (2007), Aircraft observations of dust and pollutants over northeast China: Insight into the meteorological mechanisms of transport, *J. Geophys. Res.*, *112*, D24S90, doi:10.1029/2007JD008999.

Eisinger, M., and J. P. Burrows (1998), Tropospheric sulfur dioxide observed by the ERS-2 GOME instrument, *Geophys. Res. Lett.*, *25*(22), 4177–4180, doi:10.1029/1998GL900128.

Evans, M. J., and D. J. Jacob (2005), Impact of new laboratory studies of N_2O_5 hydrolysis on global model budgets of tropospheric nitrogen oxides, ozone, and OH, *Geophys. Res. Lett.*, *32*, L09813, doi:10.1029/2005GL022469.

Fairlie, T. D., D. J. Jacob, and R. J. Park (2007), The impact of transpacific transport of mineral dust in the United States, *Atmos. Environ.*, *41*, 1251–1266, doi:10.1016/j.atmosenv.2006.09.048.

Fishman, J., et al. (2008), Remote sensing of tropospheric pollution from space, *Bull. Am. Meteorol. Soc.*, *89*, 805–821, doi:10.1175/2008BAMS2526.1.

Hains, J. C. (2007), A chemical climatology of lower tropospheric trace gases and aerosols over the mid-Atlantic region, Ph.D. dissertation, Univ. of Md. at College Park, College Park.

Heald, C. L., D. J. Jacob, R. J. Park, B. Alexander, T. D. Fairlie, R. M. Yantosca, and D. A. Chu (2006), Transpacific transport of Asian anthropogenic aerosols and its impact on surface air quality in the United States, *J. Geophys. Res.*, *111*, D14310, doi:10.1029/2005JD006847.

Herman, J. R., and E. A. Celarier (1997), Earth surface reflectivity climatology at 340–380 nm from TOMS data, *J. Geophys. Res.*, *102*(D23), 28,003–28,011, doi:10.1029/97JD02074.

Hirsch, R. M., and E. J. Gilroy (1984), Methods of fitting a straight line to data: Examples in water resources, *Water Resour. Bull.*, *20*(5), 705–711.

Hudman, R. C., et al. (2007), Surface and lightning sources of nitrogen oxides over the United States: Magnitudes, chemical evolution, and outflow, *J. Geophys. Res.*, *112*, D12S05, doi:10.1029/2006JD007912.

Inn, E. C. Y., and J. F. Vedder (1981), Measurement of stratospheric sulfur constituents, *Geophys. Res. Lett.*, *8*(1), 5–8, doi:10.1029/GL008i001p00005.

Intergovernmental Panel on Climate Change (IPCC) (2007), *Climate Change 2007: The Physical Science Basis, Contribution of Working Group I to the Fourth Assessment, Report of the Intergovernmental Panel on Climate Change*, edited by S. Solomon et al., Cambridge Univ. Press, Cambridge, U. K.

Jacob, D. J. (2000), Heterogeneous chemistry and tropospheric ozone, *Atmos. Environ.*, *34*, 2131–2159, doi:10.1016/S1352-2310(99)00462-8.

Joiner, J., and A. P. Vasilkov (2006), First results from the OMI rotational Raman scattering cloud pressure algorithm, *IEEE Trans. Geosci. Remote Sens.*, *44*(5), 1272–1282, doi:10.1109/TGRS.2005.861385.

Khokhar, M. F., C. Frankenberg, M. Van Roozendael, S. Beirle, S. Kühl, A. Richter, U. Platt, and T. Wagner (2005), Satellite observation of atmospheric SO_2 from volcanic eruptions during the time-period of 1996–2002, *Adv. Space Res.*, *36*, 879–887, doi:10.1016/j.asr.2005.04.114.

Kim, S., et al. (2007), Measurement of HO_2NO_2 in the free troposphere during the Intercontinental Chemical Transport Experiment–North America 2004, *J. Geophys. Res.*, *112*, D12S01, doi:10.1029/2006JD007676.

Krotkov, N. A., P. K. Bhartia, J. Herman, J. Slusser, G. Scott, G. Labow, A. Vasilkov, T. Eck, O. Dubovik, and B. Holben (2005), Aerosol UV absorption experiment (2002–04), 2. Absorption optical thickness, refractive index, and single scattering albedo, *Opt. Eng.*, *44*(4), 041005, doi:10.1117/1.1886819.

Krotkov, N. A., S. A. Carn, A. J. Krueger, P. K. Bhartia, and K. Yang (2006), Band residual difference algorithm for retrieval of SO_2 from the Aura Ozone Monitoring Instrument (OMI), *IEEE Trans. Geosci. Remote Sens.*, *44*(5), 1259–1266, doi:10.1109/TGRS.2005.861932.

Krotkov, N. A., et al. (2008), Validation of SO_2 retrievals from the Ozone Monitoring Instrument (OMI) over NE China, *J. Geophys. Res.*, *113*, D16S40, doi:10.1029/2007JD008818.

Krueger, A. (1983), Sighting of El Chichon sulfur dioxide clouds with the Nimbus 7 total ozone mapping spectrometer, *Science*, *220*, 1377–1379, doi:10.1126/science.220.4604.1377.

Krueger, A., L. Walter, P. Bhartia, C. Schnetzler, N. Krotkov, I. Sprod, and G. Bluth (1995), Volcanic sulfur dioxide measurements from the total ozone mapping spectrometer instruments, *J. Geophys. Res.*, *100*(D7), 14,057–14,076, doi:10.1029/95JD01222.

Kuhns, H., E. M. Knipping, and J. M. Vukovich (2005), Development of a United States–Mexico emissions inventory for the Big Bend Regional Aerosol and Visibility Observational (BRAVO) study, *J. Air Waste Manage. Assoc.*, *55*, 677–692.

Lee, C., A. Richter, J. P. Burrows, H. Lee, Y. J. Kim, Y. G. Lee, and B. C. Choi (2008a), Impact of transport of sulfur dioxide from the Asian continent on the air quality over Korea during May 2005, *Atmos. Environ.*, *42*, 1461–1475, doi:10.1016/j.atmosenv.2007.11.006.

Lee, C., A. Richter, M. Weber, and J. P. Burrows (2008b), SO_2 retrieval from SCIAMACHY using the Weighting Function DOAS (WFDOAS) technique: Comparison with standard DOAS retrieval, *Atmos. Chem. Phys.*, *8*, 17,297–17,341.

Martin, R. V., et al. (2002), An improved retrieval of tropospheric nitrogen dioxide from GOME, *J. Geophys. Res.*, *107*(D20), 4437, doi:10.1029/2001JD001027.

Martin, R. V., D. J. Jacob, K. Chance, T. P. Kurosu, P. I. Palmer, and M. J. Evans (2003a), Global inventory of nitrogen oxide emissions constrained by space-based observations of NO_2 columns, *J. Geophys. Res.*, *108*(D17), 4537, doi:10.1029/2003JD003453.

Martin, R. V., D. J. Jacob, R. M. Yantosca, M. Chin, and P. Ginoux (2003b), Global and regional decreases in tropospheric oxidants from photochemical effects of aerosols, *J. Geophys. Res.*, *108*(D3), 4097, doi:10.1029/2002JD002622.

Millet, D. B., et al. (2006), Formaldehyde distribution over North America: Implications for satellite retrievals of formaldehyde columns and isoprene emission, *J. Geophys. Res.*, *111*, D24S02, doi:10.1029/2005JD006853.

Mishchenko, M. I., J. M. Dlugach, E. G. Yanovitskij, and N. T. Zakharova (1999), Bidirectional reflectance of flat, optically thick particulate layers: An efficient radiative transfer solution and applications to snow and soil surfaces, *J. Quant. Spectrosc. Radiat. Transfer*, *63*, 409–432, doi:10.1016/S0022-4073(99)00028-X.

Newhall, C. G., and S. Self (1982), The volcanic explosivity index (VEI): An estimate of explosive magnitude for historical volcanism, *J. Geophys. Res.*, *87*(C2), 1231–1238, doi:10.1029/JC087iC02p01231.

Olivier, J. G. J., J. J. M. Berdowski, J. A. H. W. Peters, J. Bakker, A. J. H. Visschedijk, and J. P. J. Bloos (2001), Applications of EDGAR including a description of EDGAR 3.2: Reference database with trend data for 1970–1995, *RIVM Rep. 773301001*, Natl. Inst. of Public Health and the Environ., Bilthoven.

Palmer, P. I., D. J. Jacob, K. Chance, R. V. Martin, R. J. D. Spurr, T. P. Kurosu, I. Bey, R. Yantosca, A. Fiore, and Q. Li (2001), Air mass factor formulation for spectroscopic measurements from satellites: Application to formaldehyde retrievals from the Global Ozone Monitoring Experiment, *J. Geophys. Res.*, *106*(D13), 14,539–14,550, doi:10.1029/2000JD900772.

Park, R. J., D. J. Jacob, M. Chin, and R. V. Martin (2003), Sources of carbonaceous aerosols over the United States and implications for natural visibility, *J. Geophys. Res.*, *108*(D12), 4355, doi:10.1029/2002JD003190.

Park, R. J., D. J. Jacob, B. D. Field, and R. M. Yantosca (2004), Natural and transboundary pollution influences on sulphate-nitrate ammonium aerosols in the United States: Implications for policy, *J. Geophys. Res.*, *109*, D15204, doi:10.1029/2003JD004473.

Patterson, E. M., D. A. Gillet, and B. H. Stockton (1977), Complex index of refraction between 300 and 700 nm for Saharan aerosol, *J. Geophys. Res.*, *82*(21), 3153–3160, doi:10.1029/JC082i021p03153.

Prata, A. J., S. A. Carn, A. Stohl, and J. Kerkmann (2007), Long range transport and fate of a stratospheric volcanic cloud from Soufriere Hills volcano, Montserrat, *Atmos. Chem. Phys.*, *7*, 5093–5103.

Pyle, D. M., P. D. Beattie, and G. J. S. Bluth (1996), Sulphur emissions to the stratosphere from explosive volcanic eruptions, *Bull. Volcanol.*, *57*, 663–671, doi:10.1007/s004450050119.

Richter, A., and J. P. Burrows (2002), Tropospheric NO_2 from GOME measurements, *Adv. Space Res.*, *29*, 1673–1683, doi:10.1016/S0273-1177(02)00100-X.

Richter, A., V. Eyring, J. P. Burrows, H. Bovensmann, A. Lauer, B. Sierk, and P. J. Crutzen (2004), Satellite measurements of NO_2 from international shipping emissions, *Geophys. Res. Lett.*, *31*, L23110, doi:10.1029/2004GL020822.

Richter, A., F. Wittrock, and J. P. Burrows (2006), SO_2 Measurements with SCIAMACHY, paper presented at Atmospheric Science Conference 2006, Eur. Space Agency, Frascati, Italy.

Ryerson, T. B., et al. (1998), Emissions lifetimes and ozone formation in power plant plumes, *J. Geophys. Res.*, *103*(D17), 22,569–22,583, doi:10.1029/98JD01620.

Sauvage, B., R. V. Martin, A. van Donkelaar, X. Liu, K. Chance, L. Jaeglé, P. I. Palmer, S. Wu, and T.-M. Fu (2007), Remote sensed and in situ constraints on processes affecting tropical tropospheric ozone, *Atmos. Chem. Phys.*, *7*, 815–838.

Simkin, T., and L. Siebert (1994), *Volcanoes of the World*, 2nd ed., 368 pp., Geosci. Press, Tucson, Ariz.

Singh, H. B., W. H. Brune, J. H. Crawford, D. J. Jacob, and P. B. Russell (2006), Overview of the summer 2004 Intercontinental Chemical Transport Experiment–North America (INTEX-A), *J. Geophys. Res.*, *111*, D24S01, doi:10.1029/2006JD007905.

Singh, H. B., W. H. Brune, J. H. Crawford, F. Flocke, and D. J. Jacob (2009), Chemistry and transport of pollution over the Gulf of Mexico and the Pacific: Spring 2006 INTEX-B Campaign overview and first results, *Atmos. Chem. Phys.*, *9*, 2301–2318.

Sinyuk, A., O. Torres, and O. Dubovik (2003), Combined use of satellite and surface observations to infer the imaginary part of refractive index of Saharan dust, *Geophys. Res. Lett.*, *30*(2), 1081, doi:10.1029/2002GL016189.

Spurr, R. J. D. (2002), Simultaneous derivation of intensities and weighting functions in a general pseudo-spherical discrete ordinate radiative transfer

treatment, *J. Quant. Spectrosc. Radiat. Transfer*, *75*, 129–175, doi:10.1016/S0022-4073(01)00245-X.

Spurr, R. J. D., T. P. Kurosu, and K. V. Chance (2001), A linearized discrete ordinate radiative transfer model for atmospheric remote-sensing retrieval, *J. Quant. Spectrosc. Radiat. Transfer*, *68*, 689–735, doi:10.1016/S0022-4073(00)00055-8.

Streets, D. G., and S. T. Waldhoff (2000), Present and future emissions of air pollutants in China: SO_2, NO_x, and CO, *Atmos. Environ.*, *34*, 363–374, doi:10.1016/S1352-2310(99)00167-3.

Taubman, B. F., J. C. Hains, A. M. Thompson, L. T. Marufu, B. G. Doddridge, J. W. Stehr, C. A. Piety, and R. R. Dickerson (2006), Aircraft vertical profiles of trace gas and aerosol pollution over the mid-Atlantic United States: Statistics and meteorological cluster analysis, *J. Geophys. Res.*, *111*, D10S07, doi:10.1029/2005JD006196.

Thomas, W., T. Erbertseder, T. Ruppert, M. Van Roozendael, J. Verdebout, D. Balis, C. Meleti, and C. Zerefos (2005), On the retrieval of volcanic sulfur dioxide emissions from GOME backscatter measurements, *J. Atmos. Chem.*, *50*, 295–320, doi:10.1007/s10874-005-5544-1.

Torres, O., and P. K. Bhartia (1999), Impact of tropospheric aerosol absorption on ozone retrieval from backscattered ultraviolet measurements, *J. Geophys. Res.*, *104*(D17), 21,569–21,577.

Torres, O., A. Tanskanen, B. Veihelmann, C. Ahn, R. Braak, P. K. Bhartia, P. Veefkind, and P. Levelt (2007), Aerosols and surface UV products from Ozone Monitoring Instrument observations: An overview, *J. Geophys. Res.*, *112*, D24S47, doi:10.1029/2007JD008809.

Vandaele, A. C., P. C. Simon, J. M. Guilmot, M. Carleer, and R. Colin (1994), SO_2 absorption cross section measurement in the UV using a Fourier transform spectrometer, *J. Geophys. Res.*, *99*(D12), 25,599–25,605, doi:10.1029/94JD02187.

van Donkelaar, A., et al. (2008), Analysis of aircraft and satellite measurements from the Intercontinental Chemical Transport Experiment (INTEX-B) to quantify long-range transport of East Asian sulfur to Canada, *Atmos. Chem. Phys.*, *8*, 2999–3014.

Van Roozendael, M., V. Soevijanta, C. Fayt, and J.-C. Lamvert (2002), Investigation of DOAS issues affecting the accuracy of the GDP version 3.0 total ozone product, in *ERS-2 GOME GDP 3.0 Implementation and Delta Validation*, pp. 97–129, Eur. Space Agency, Frascati, Italy.

Vasilkov, A., J. Joiner, R. Spurr, P. K. Bhartia, P. Levelt, and G. Stephens (2008), Evaluation of the OMI cloud pressures derived from rotational Raman scattering by comparisons with other satellite data and radiative transfer simulations, *J. Geophys. Res.*, *113*, D15S19, doi:10.1029/2007JD008689.

Vountas, M., V. V. Rozanov, and J. P. Burrows (1998), Ring effect: Impact of rotational Raman scattering on radiative transfer in Earth's atmosphere, *J. Quant. Spectrosc. Radiat. Transfer*, *60*, 943–961, doi:10.1016/S0022-4073(97)00186-6.

Wang, C., J. J. Corbett, and J. Firestone (2008), Improving spatial representation of global ship emissions inventories, *Environ. Sci. Technol.*, *42*, 193–199, doi:10.1021/es0700799.

Wang, P., P. Stammes, R. van der A, G. Pinardi, and M. van Roozendael (2008), FRESCO+: An improved O_2 A-band cloud retrieval algorithm for tropospheric trace gas retrievals, *Atmos. Chem. Phys.*, *8*, 6565–6576.

Weber, M., L. N. Lamsal, and J. P. Burrows (2007), Improved SCIAMACHY total ozone retrieval: Steps towards homogenizing long-term total ozone datasets from GOME, SCIAMACHY, and GOME2, paper presented at 2007 ESA ENVISAT Symposium, Eur. Space Agency, Montreux, Switzerland.

Wenig, M. O., A. M. Cede, E. J. Bucsela, E. A. Celarier, K. F. Boersma, J. P. Veefkind, E. J. Brinksma, J. F. Gleason, and J. R. Herman (2008), Validation of OMI tropospheric NO_2 column densities using direct-sun mode Brewer measurements at NASA Goddard Space Flight Center, *J. Geophys. Res.*, *113*, D16S45, doi:10.1029/2007JD008988.

Yang, K., N. A. Krotkov, A. J. Krueger, S. A. Carn, P. K. Bhartia, and P. F. Levelt (2007), Retrieval of large volcanic SO_2 columns from the Aura Ozone Monitoring Instrument: Comparison and limitations, *J. Geophys. Res.*, *112*, D24S43, doi:10.1029/2007JD008825.

Zhang, Q., et al. (2009), Asian emissions in 2006 for the NASA INTEX-B mission, *Atmos. Chem. Phys. Discuss.*, *9*, 4081–4139.

J. S. Holloway, Cooperative Institute for Research in Environmental Science, University of Colorado at Boulder, 216 UCB, Boulder, CO 80309-0216, USA.

L. G. Huey, School of Earth and Atmospheric Sciences, Georgia Institute of Technology, 311 Ferst Dr., Atlanta, GA 30332-0340, USA.

N. Krotkov, Goddard Earth Sciences and Technology Center, University of Maryland, Baltimore County, 5523 Research Park Dr., Baltimore, MD 21228, USA.

C. Lee, R. V. Martin, G. O'Byrne, and A. van Donkelaar, Department of Physics and Atmospheric Science, Dalhousie University, 6310 Coburg Rd., Halifax, NS B3H 3J5, Canada. (chulkyu.lee@dal.ca)

A. Richter, Institute of Environmental Physics and Remote Sensing, University of Bremen, 1 Otto-Hahn-Allee, Bremen D-28359, Germany.